An Information-Theoretic Characterization of MIMO-FAS: Optimization, Diversity-Multiplexing Tradeoff and q-Outage Capacity

Wee Kiat New, *Member, IEEE*, Kai-Kit Wong, *Fellow, IEEE*, Hao Xu, *Member, IEEE*,
Kin-Fai Tong, *Fellow, IEEE*, *and* Chan-Byoung Chae, *Fellow, IEEE*

Abstract—Multiple-input multiple-output (MIMO) system has been the defining mobile communications technology in recent generations. With the ever-increasing demands looming towards the sixth generation (6G), we are in need of additional degrees of freedom that deliver further gains beyond MIMO. To this goal, fluid antenna system (FAS) has emerged as a new way to obtain spatial diversity using reconfigurable position-switchable antennas. Considering the case with more than one ports activated on a 2D fluid antenna surface at both ends, we take the information-theoretic approach to study the achievable performance limits of the MIMO-FAS. First of all, we propose a suboptimal scheme, referred to as QR MIMO-FAS, to maximize the rate at high signal-to-noise ratio (SNR) via joint port selection, transmit and receive beamforming and power allocation. We then derive the optimal diversity and multiplexing tradeoff (DMT) of MIMO-FAS. From the DMT, we highlight that MIMO-FAS outperforms traditional MIMO antenna systems. Further, we introduce a new metric, namely q-outage capacity, which can jointly consider rate and outage probability. Through this metric, our results indicate that MIMO-FAS surpasses traditional MIMO greatly.

Index Terms—6G, Diversity and multiplexing tradeoff, Fluid antenna system, MIMO, Outage capacity.

I. INTRODUCTION

A. Background

SIXTH-GENERATION (6G) mobile communication seeks to push the key performance indicators (KPIs) way beyond what the current fifth generation (5G) promises to offer. Such upgrade will require new technologies that can achieve more from the same amount of bandwidth. Presently, the dominating technology has been multiple-input multiple-output (MIMO), which also comes in the form of multiuser MIMO and massive MIMO. In 6G, the desire is to exceed MIMO [1], [2].

To achieve this very ambitious goal, one emerging idea is fluid antenna system (FAS) [3]. FAS represents any software-controllable fluidic, conductive or dielectric structure that can adjust its shape and position to reconfigure the gain, radiation pattern, operating frequency and other radiation characteristics. This is now feasible, thanks to the recent advances in utilizing flexible conductive materials such as liquid metals or ionized solutions [4], switchable pixels [5], [6], and stepper motors for antennas [7], [8]. The concept of fluid antenna includes all forms of movable and non-movable flexible-position antennas.

Unlike traditional antenna that is placed at a fixed location, fluid antenna is able to switch its location almost instantly in a limited space. The most basic single fluid antenna consists of one radio frequency (RF)-chain and N preset locations (also known as ports) that are distributed in a given space [3]. The radiating element of the fluid antenna can switch its position to obtain a higher rate, lower outage probability, less interference and other desirable performance gains depending on the applications. As the ports can be placed closely to each other, the channels of these ports are strongly correlated and thus spatial correlation plays a crucial role in FAS.

The main implementation designs for FAS are: i) liquid-based fluid antenna and ii) RF pixel-based fluid antenna. In the liquid-based fluid antenna, each liquid droplet can precisely switch its position by controlling the electric field using the thin conductive lines on top of the dielectric layer while other technology may use an electronically controlled pump to shift the position of a fluid radiating element in a tube. On the other hand, in the RF pixel-based fluid antenna, the RF pixels can be turned on-and-off instantly regardless of the surface area. One or several pixels when on, form an antenna port for transmission or reception like a standard antenna. Besides, each activated port is connected to an RF-chain, operating like a conventional antenna. In short, the basic principle of FAS is to exploit the dynamic nature of fluid antenna to achieve ultimate flexibility for diversity and multiplexing gains.[1]

Due to its unprecedented benefits, single-user, single-input single-output (SISO)-FAS has recently been investigated under different scenarios and assumptions. Specifically, as the number of ports increases, [9] showed that the outage probability of FAS could be reduced drastically while [10] demonstrated that FAS could significantly improve the ergodic capacity.

---

[1]It is worth pointing out that FAS does not necessarily use 'fluid' materials for antenna and in wireless communications that requires adaptation in time of milliseconds or less, reconfigurable pixels are more relevant.

Motivated by these works, [11] derived the level crossing rate, [12] devised a port selection algorithm by observing the channels of a few ports, [13] investigated the performance of FAS over general correlated channels and [14] analyzed the outage probability of FAS for Terahertz communications while selection combining and maximum gain combining were further considered. Optimistic results were obtained in these works but it was illustrated in [15] that the outage probability of FAS could only be reduced to a floor when a more accurate spatial correlation model was adopted. The recent work [16] explained such limitations at an intuitive level and revealed that the performance of FAS was generally determined by the available space. Furthermore, only in certain cases might FAS achieve a similar outage probability as compared to the classical maximal ratio combining (MRC) system.

The unique ability of switching the antenna position finely in FAS can also be exploited to mitigate interference, which would be impractical in traditional antenna selection systems. Recently, [17] investigated orthogonal multiple access to serve multiple users with fluid antennas while [18] used a space division multiple access approach to minimize the user transmit power. Nevertheless, an arguably more interesting idea is the fluid antenna multiple access (FAMA) scheme [19] where the rationale is to exploit the moment of deep fades in the spatial domain to alleviate inter-user interference. FAMA is classified into slow FAMA and fast FAMA in which the former switches its port when the channel changes [20] and the latter switches its port on a symbol-by-symbol basis [21]. Most recently, the outage probability for two-user FAMA was revisited in [22].

In summary, FAS has shown promises but much is still not well understood. For example, the performance of FAS itself can be lifted if more than one ports are activated. For a point-to-point communication channel, we refer to the system where both ends are equipped with a multi-port FAS, as MIMO-FAS which is also known as fluid MIMO or flexible MIMO in [3]. Note that multiple ports can also be activated in a two dimensional (2D) surface using liquid-based fluid antenna or RF pixel-based fluid antenna. The schematics of the MIMO-FAS designs were discussed in [3]. Compared to a traditional MIMO antenna selection system in which the number of antennas is limited in a given surface (at least half wavelength separation between the antennas) and the antennas are fixed in positions, MIMO-FAS is distinct in the sense that the positions of the radiating elements can be dynamically and finely adjusted and that the number of preset locations (i.e., ports) within a given surface can be arbitrarily large, which yields additional gains. Note that FAS has also been proposed for multiple access recently [20]–[22], where the fine resolution of FAS is absolutely essential and conventional antenna selection would be unable to cope.

It is anticipated that the capacity and reliability of MIMO-FAS will be improved over the SISO counterpart. In fact, a related work showed that the capacity of a movable antenna system (which can be interpreted as MIMO-FAS with movable fluid antennas) could be improved up to 30.3% as compared to traditional MIMO systems [23]. In the study, however, spatial correlation due to rich scattering between the antenna positions was not considered. More importantly, the optimal diversity

and multiplexing tradeoff (DMT) of MIMO-FAS is unknown.

In information theory, the optimal DMT can be employed as a unified framework to compare the performance of different multiple-antenna systems [24]. More concretely, it focuses on the asymptotic high signal-to-noise ratio (SNR) regime and a scheme is then said to achieve a multiplexing gain of r and a diversity gain of $d(r)$ if the rate of the system scales like $r \log \mathrm{SNR}$ and its outage probability decays like $\mathrm{SNR}^{-d(r)}$. It is known that r cannot exceed the total degrees of freedom of the channel and $d(0)$ is limited by the maximal diversity gain, i.e., total number of independent channels. In between the two extremes, a system must tradeoff each type of gains.

B. Contributions

Motivated by the above, this paper analyzes the performance of MIMO-FAS with the goal of gaining useful insights for designing an efficient MIMO-FAS. To this end, we first develop a system model of MIMO-FAS while taking into account of the spatial correlation effect. To characterize the performance limits of MIMO-FAS, we consider a rich scattering environment since it is well known that multipath can help to improve the diversity and multiplexing gains.[2] We then propose a suboptimal scheme that maximizes the rate of MIMO-FAS through joint port selection, transmit and receive beamforming and power allocation at high SNR. Based on this scheme, we derive the optimal DMT of MIMO-FAS to reveal the fundamental limits of MIMO-FAS from an information-theoretic viewpoint. From the analytical results, we further study the effects of different MIMO-FAS parameters and reveal the superiority of MIMO-FAS over traditional MIMO and MIMO antenna selection in terms of DMT. In addition, we introduce a new metric, referred to as q-outage capacity, to showcase the benefits of MIMO-FAS. Our main contributions are summarized as follows:

- We develop a system model for MIMO-FAS with a 2D fluid antenna surface at both ends while taking into account of the spatial correlation of the ports. In particular, we employ a simple yet accurate channel model that considers the spatial correlation in a three-dimensional (3D) scattering environment. Based on this channel model, we introduce several system parameters such as active ports, beamforming matrices and power allocation. The achievable rate of MIMO-FAS is then derived where its expression resembles the rate of a traditional MIMO system.

- Also, we formulate a non-convex optimization problem to maximize the rate of MIMO-FAS via joint port selection, transmit and receive beamforming and power allocation. We show that the global optimal solution can be obtained using an exhaustive search, singular value decomposition (SVD) and waterfilling power allocation, at the expense of a non-polynomial time complexity. To

---

[2]Note that rich scattering can help to improve the performance of any MIMO systems. This includes MIMO-FAS, traditional MIMO and MIMO antenna selection. Therefore, if the number of scatterers is small, one may further consider using a reconfigurable intelligent surface to create artificial scatterers to improve the performance of any MIMO systems.

reduce the time complexity, we propose the QR MIMO-FAS scheme that maximizes the rate of MIMO-FAS at high SNR via suboptimal port selection, beamforming and power allocation. It is shown that QR MIMO-FAS has a polynomial time complexity.

- Furthermore, we derive the outer bound of the DMT of MIMO-FAS. By using the outer bound and QR MIMO-FAS, we obtain the optimal DMT of MIMO-FAS. In this process, we prove that the spatial correlation matrix $\boldsymbol{J}_s$ can be represented by a finite-size matrix $\boldsymbol{J}_{\text{red}}^s$ even if the number of ports increases to infinity. Afterwards, we propose methods to estimate the size of $\boldsymbol{J}_{\text{red}}^s$ and linearly transform between $\boldsymbol{J}_s$ and $\boldsymbol{J}_{\text{red}}^s$ with proof of certificates.
- Extensive results are provided to highlight the effects of several MIMO-FAS parameters. In the discussions, we provide useful insights for designing an efficient MIMO-FAS. Although MIMO-FAS provides rate improvements over the traditional MIMO antenna systems, we highlight that the superiority of MIMO-FAS actually lies in the diversity gain. Specifically, the diversity gain of MIMO-FAS for a fixed r is much greater than that of MIMO and MIMO antenna selection if the total number of active ports or antennas is the same.
- Finally, we introduce a new performance metric, referred to as q-outage capacity, that jointly considers both rate and outage probability. We show that MIMO-FAS outperforms the traditional MIMO and MIMO antenna selection in terms of q-outage capacity. This result suggests that MIMO-FAS is more reliable in delivering high data rate transmission than the traditional MIMO systems.

C. Organization and Notations

The remainder of this paper is organized as follows. Section II introduces the system model of MIMO-FAS. Section III details the proposed QR MIMO-FAS scheme that maximizes its rate at high SNR. The optimal DMT of MIMO-FAS is analyzed in Section IV. Section V presents the numerical results to compare MIMO-FAS with the traditional MIMO systems and we conclude the paper in Section VI.

Throughout this paper, scalar variables are denoted by italic letters (e.g., c), vectors are denoted by boldface italic small letters (e.g., $\boldsymbol{c}$) and matrices are denoted by boldface italic capital letters (e.g., $\boldsymbol{C}$). Additionally, $(\cdot)^T$ denotes transpose, $(\cdot)^H$ denotes conjugate transpose while $\det(\cdot)$, $\text{rank}(\cdot)$ and $\text{trace}(\cdot)$ represent the determinant, rank and trace of a matrix, respectively. Moreover, $|\cdot|$, $\|\cdot\|_2$ and $\|\cdot\|_F$ denote the absolute, Euclidean norm and Frobenius norm operations, respectively. Furthermore, we use $\log(\cdot)$ to denote logarithm with base 2, $[\cdot]_c^+$ outputs the argument that is lower bounded by c, $\min\{\cdot\}$ and $\max\{\cdot\}$ denote the minimum and maximum value of the argument, respectively. $\mathbb{E}[\cdot]$ returns the expected value of the input random quantity, and $\otimes$ denotes the Kronecker product. Finally, $\boldsymbol{e}_k$ represents an all-zero vector except the k-th entry being unity, $\text{diag}(\cdot)$ denotes a diagonal matrix whose diagonal entries are the inputs, and $(\cdot)^\dagger$ denotes the pseudoinverse of an input matrix. To help readers follow the mathematical contents, the meanings of the key variables are listed in Table I.

Table I: The meanings of key notations.

Notation	Meaning
$\boldsymbol{A}$	Activation port matrices at both of the transmitter and receiver sides
$\boldsymbol{A}_s$	Activation port matrix at side s
C_{sys}^q	q-outage capacity of a system
$d(r)$	Diversity gain for r multiplexing gain
$\boldsymbol{G}$	Circularly symmetric complex Gaussian matrix with i.i.d. entries
$\boldsymbol{H}$	Complex channels of MIMO-FAS
$\bar{\boldsymbol{H}}$	Complex channels of the activated ports
$\boldsymbol{H}_a$	Partial channels of the active ports
$\boldsymbol{H}_i$	Partial channels of the inactive ports
$\boldsymbol{J}_s$	Spatial correlation matrix at side s
$\hat{\boldsymbol{J}}_s$	Approximated matrix of $\boldsymbol{J}_s$
$\boldsymbol{J}_{\text{red}}^s$	Full rank spatial correlation matrix at side s
$\boldsymbol{K}$	Input covariance
n_s	Total number of active ports
$n_{\max}/n_{\min}$	Maximum/minimum of n_{rx} and n_{tx}
$N_{\max}/N_{\min}$	Maximum/minimum of N_{rx} and N_{tx}
N_s	Total number of ports at side s
N_i^s	Number of ports in the i-th dimension at side s
N_s'	Rank of $\boldsymbol{J}_{\text{red}}^s$
$N_{\min}'$	Minimum of N_{rx}' and N_{tx}'
$P_{\text{sys}}^{\text{out}}(\text{SNR}, r)$	Outage probability of a system in terms of $r \log \text{SNR}$
$\bar{P}_{\text{sys}}^{\text{out}}(\text{SNR}, q)$	Outage probability of a system for a fixed q-transmission rate
$\boldsymbol{P}$	Power allocation matrix
r	Multiplexing gain
$R_{\text{sys}}(\text{SNR})$	Rate of a system for a given SNR
$s \in \{tx, rx\}$	Subscript/superscript to denote the transmit/receiver side
SNR	Transmit SNR
$\boldsymbol{v}_l^s$	Certificate between the linear transformation of $\boldsymbol{J}_s^{(l)}$ and $\boldsymbol{J}_{\text{sub}}^{(l-1)}$
W_s	Total area of the fluid antenna at side s
W_i^s	Length of the fluid antenna in the i-th dimension at side s
$\boldsymbol{W}$	Transmit and receive beamforming matrices
$\boldsymbol{W}_s$	Beamforming matrix at s side
λ	Wavelength of the carrier frequency
$\boldsymbol{\Lambda}_s$	Matrix whose diagonal entries are the eigenvalues of $\boldsymbol{J}_s$
$\boldsymbol{\Sigma}$	Matrix whose diagonal entries are singular values of $\boldsymbol{H}$
$\bar{\boldsymbol{\Sigma}}$	Matrix whose diagonal entries are singular values of $\bar{\boldsymbol{H}}$
$\boldsymbol{\Omega}$	Special matrix used for port optimization

II. SYSTEM MODEL

As illustrated in Fig. 1, we consider a point-to-point wireless communication channel in which the transmitter and receiver are equipped with a fluid antenna. To facilitate our discussions, we use the subscript/superscript s to denote the parameters at the transmitter or receiver as tx or rx, respectively, i.e., $s \in \{tx, rx\}$. We assume that the fluid antenna takes up a 2D space with an area of W_s and has N_s ports spread uniformly over the 2D space. A grid structure is considered where N_i^s ports are uniformly distributed along a linear space of length λW_i^s for $i \in \{1, 2\}$, so that $N_s = N_1^s \times N_2^s$ and $W_s = \lambda W_1^s \times \lambda W_2^s$, where λ is the wavelength of the carrier frequency. In this MIMO-FAS, the transmitter and receiver can only activate n_s out of N_s ports. Note that for SISO-FAS, $n_s = 1, \forall s$.

Considering a 3D environment under rich scattering, the spatial correlation between the (n_1^s, n_2^s)-th port and the
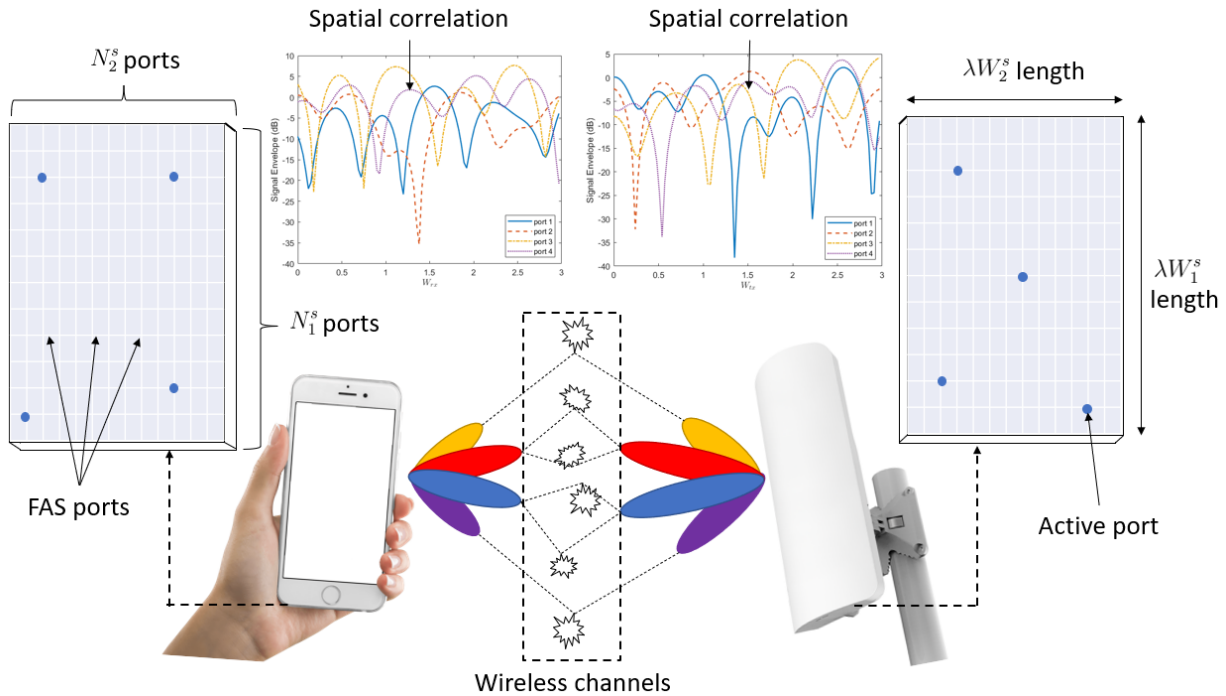
Figure 1: A schematic of point-to-point MIMO-FAS.

$(\tilde{n}_1^s, \tilde{n}_2^s)$-th port is given by

$$J^s_{\left(n_1^s, n_2^s\right), \left(\tilde{n}_1^s, \tilde{n}_2^s\right)}$$
$$= j_0\left(2\pi\sqrt{\left(\frac{|n_1^s - \tilde{n}_1^s|}{N_1^s - 1}W_1^s\right)^2 + \left(\frac{|n_2^s - \tilde{n}_2^s|}{N_2^s - 1}W_2^s\right)^2}\right), \quad (1)$$

where $j_0\left(\cdot\right)$ is the spherical Bessel function of the first kind.[3] A detailed proof can be found in Appendix I. As seen in (1), it is cumbersome to label a port in 2D. To simplify our notations, we use the function $\mathrm{map} : \mathbb{R}^2 \to \mathbb{R}$, e.g., $\mathrm{map}\left(n_1^s, n_2^s\right) = l_s$, where $l_s \in \{1, \ldots, N_s\}$.

Using the mapping function, we can express the spatial correlation matrix $\boldsymbol{J}_s$ as

$$\boldsymbol{J}_s = \begin{bmatrix} J_{1,1}^s & J_{1,2}^s & \cdots & J_{1,N_s}^s \\ J_{2,1}^s & J_{2,2}^s & \cdots & J_{2,N_s}^s \\ \vdots & \vdots & \ddots & \vdots \\ J_{N_s,1}^s & J_{N_s,2}^s & \cdots & J_{N_s,N_s}^s \end{bmatrix}, \quad (2)$$

where J_{k_s,l_s}^s is the spatial correlation of the k_s-th and the l_s-th port at side s, and k_s and l_s are the labels after mapping. Since $J_{k_s,l_s}^s = J_{l_s,k_s}^s$, (2) can be decomposed into $\boldsymbol{J}_s = \boldsymbol{U}_s \boldsymbol{\Lambda}_s \boldsymbol{U}_s^H$ where $\boldsymbol{U}_s$ is an $N_s \times N_s$ matrix whose l-th column (i.e., $\boldsymbol{u}_l^s$) is the eigenvector of $\boldsymbol{J}_s$ and $\boldsymbol{\Lambda}_s = \mathrm{diag}\left(\lambda_1^s, \ldots, \lambda_{N_s}^s\right)$ is an $N_s \times N_s$ diagonal matrix whose l-th diagonal entries are the corresponding eigenvalues of $\boldsymbol{u}_l^s$. Without loss of generality, we assume that the values of the eigenvalues in $\boldsymbol{\Lambda}_s$ are in descending order, i.e., $\lambda_1^s \geq \cdots \geq \lambda_{N_s}^s$. Note that $\boldsymbol{U}_s \boldsymbol{\Lambda}_s \boldsymbol{U}_s^H$ is computed independently for each $s \in \{tx, rx\}$.

Given $\boldsymbol{U}_s$ and $\boldsymbol{\Lambda}_s$ for $\forall s$, the complex channel of MIMO-FAS can be modelled as

$$\boldsymbol{H} = \delta\,\boldsymbol{U}_{rx}\sqrt{\boldsymbol{\Lambda}_{rx}}\boldsymbol{G}\sqrt{\boldsymbol{\Lambda}_{tx}^H}\boldsymbol{U}_{tx}^H, \quad (3)$$

where $\boldsymbol{G} = \left[\boldsymbol{g}_1, \ldots, \boldsymbol{g}_{N_{tx}}\right]$, $\boldsymbol{g}_l = \left[g_{1,l}, \ldots, g_{N_{rx},l}\right]^T$, $g_{k,l} = x_{k,l} + jy_{k,l}$, and $x_{k,l}, y_{k,l}$ are independent Gaussian random variables with zero mean and variance of $\frac{1}{2}$, $\forall k, l$, and δ^2 is the path loss. Letting $\boldsymbol{h}_{\mathrm{vec}} = \mathrm{vec}\left(\boldsymbol{H}\right)$, the covariance of $\boldsymbol{h}_{\mathrm{vec}}$ is $\delta^2\left(\boldsymbol{J}_{tx}^T \otimes \boldsymbol{J}_{rx}\right)$, where $\boldsymbol{J}_{tx}^T \otimes \boldsymbol{J}_{rx}$ is the spatial correlation matrix between the transmit and receive ports.[4]

Next, we denote the activation port matrices at the transmitter and receiver, respectively, as $\boldsymbol{A}_{tx} = \left[\boldsymbol{a}_1^{tx}, \ldots, \boldsymbol{a}_{n_{tx}}^{tx}\right]$ and $\boldsymbol{A}_{rx} = \left[\boldsymbol{a}_1^{rx}, \ldots, \boldsymbol{a}_{n_{rx}}^{rx}\right]^T$, where $\boldsymbol{a}_l^{tx}$ and $\boldsymbol{a}_l^{rx}$ are standard basis vector (i.e., $\boldsymbol{a}_l^s \in \{\boldsymbol{e}_1, \ldots, \boldsymbol{e}_{N_s}\}$). Since only distinct n_s ports can be activated at a time, we have $\boldsymbol{a}_k^{tx} \neq \boldsymbol{a}_l^{tx}$ and $\boldsymbol{a}_k^{rx} \neq \boldsymbol{a}_l^{rx}$ if $k \neq l$. Let us further denote $\boldsymbol{W}_{tx}$ and $\boldsymbol{W}_{rx}$ as the transmit and receive beamforming matrices, with the constraint $\|\boldsymbol{W}_s\|_2 = 1$. Then the receive signals of MIMO-FAS can be rewritten as

$$\boldsymbol{W}_{rx}\boldsymbol{A}_{rx}\boldsymbol{Y} = \boldsymbol{W}_{rx}\boldsymbol{A}_{rx}\boldsymbol{H}\boldsymbol{A}_{tx}\boldsymbol{W}_{tx}\boldsymbol{x} + \boldsymbol{W}_{rx}\boldsymbol{A}_{rx}\boldsymbol{w} \quad (4)$$
$$\Rightarrow \tilde{\boldsymbol{Y}} = \tilde{\boldsymbol{H}}\boldsymbol{x} + \tilde{\boldsymbol{w}}, \quad (5)$$

where $\boldsymbol{x}$ is the information signal and $\boldsymbol{w}$ is the additive white Gaussian noise with zero mean and identity covariance. In (5), we defined $\tilde{\boldsymbol{Y}} \triangleq \boldsymbol{W}_{rx}\boldsymbol{A}_{rx}\boldsymbol{Y}$, $\tilde{\boldsymbol{H}} \triangleq \boldsymbol{W}_{rx}\boldsymbol{A}_{rx}\boldsymbol{H}\boldsymbol{A}_{tx}\boldsymbol{W}_{tx}$ and $\tilde{\boldsymbol{w}} \triangleq \boldsymbol{W}_{rx}\boldsymbol{A}_{rx}\boldsymbol{w}$. For ease of expositions, we denote

---

[3]Note that (1) can be reduced to a 1D fluid antenna under 2D scattering environments by setting $N_1^s = 1$ and $\frac{0}{0} \triangleq 0$ and replacing $j_0\left(\cdot\right)$ by $J_0\left(\cdot\right)$ where $J_0\left(\cdot\right)$ is the Bessel function of the first kind.

[4]Due to the port spatial correlation, it can be shown that only a small number of observed ports/training is required to obtain the full channel state information regardless of the number of ports of the FAS [25]. Machine learning techniques have also been proposed to address the channel estimation problem for port selection in FAS, e.g., [20].

$\boldsymbol{A} = [\boldsymbol{A}_{tx}, \boldsymbol{A}_{rx}]$, $\boldsymbol{W} = [\boldsymbol{W}_{tx}, \boldsymbol{W}_{rx}]$, $\bar{\boldsymbol{H}} = \boldsymbol{A}_{rx} \boldsymbol{H} \boldsymbol{A}_{tx}$ and $\boldsymbol{K} = \boldsymbol{W}_{tx} \boldsymbol{P} \boldsymbol{W}_{tx}^H$ where $\boldsymbol{K}$ is the input covariance and $\boldsymbol{P} = \mathbb{E}\left[\boldsymbol{x}\boldsymbol{x}^H\right]$ is the power allocation matrix. Then, the rate of MIMO-FAS is given by

$$R\left(\boldsymbol{A}, \boldsymbol{W}, \boldsymbol{P}\right) = \log \det \left(\boldsymbol{I} + \bar{\boldsymbol{H}} \boldsymbol{K} \bar{\boldsymbol{H}}^H\right), \qquad (6)$$

where $\mathrm{trace}\left(\boldsymbol{K}\right) \leq \mathrm{SNR}$ and SNR is the transmit SNR.

III. QR MIMO-FAS: Suboptimal Port Selection, Beamforming and Power Allocation

In this section, we aim to maximize the rate of the MIMO-FAS via joint optimal port selection, beamforming and power allocation. The optimization problem is formulated as

$$\max_{\boldsymbol{A}, \boldsymbol{W}, \boldsymbol{P}} \; R\left(\boldsymbol{A}, \boldsymbol{W}, \boldsymbol{P}\right) \qquad (7a)$$

$$\text{s.t.} \quad \boldsymbol{a}_l^s \in \{e_1, \ldots, e_{N_s}\}, s \in \{rx, tx\}, \forall l, \qquad (7b)$$

$$\boldsymbol{a}_k^{tx} \neq \boldsymbol{a}_l^{tx}, \text{ if } k \neq l, \qquad (7c)$$

$$\boldsymbol{a}_k^{rx} \neq \boldsymbol{a}_l^{rx}, \text{ if } k \neq l, \qquad (7d)$$

$$\|\boldsymbol{W}_{tx}\|_2 = \|\boldsymbol{W}_{rx}\|_2 = 1, \qquad (7e)$$

$$\mathrm{trace}\left(\boldsymbol{K}\right) \leq \mathrm{SNR}. \qquad (7f)$$

Note that (7) is a non-convex optimization problem because i) the optimization variables are mutually coupled and ii) its domain is non-convex. A systematic way to solve this problem is to employ an exhaustive search [26], SVD and waterfilling power allocation [27]. In particular, the maximum rate of MIMO-FAS can be computed via SVD and waterfilling power allocation over $\begin{pmatrix} N_{tx} \\ n_{tx} \end{pmatrix} \times \begin{pmatrix} N_{rx} \\ n_{rx} \end{pmatrix}$ port combinations.[5] Nevertheless, such a method requires a non-polynomial time complexity of $\mathcal{O}\left(N_{tx}^{n_{tx}} N_{rx}^{n_{rx}}\right)$ which is prohibitively high.

To reduce the time complexity, we propose a suboptimal scheme, namely QR MIMO-FAS, to maximize the rate of MIMO-FAS in the high SNR regime. This scheme is useful for analyzing the DMT of MIMO-FAS. In the proposed scheme, we decouple (7) into two subproblems: i) optimal port selection and ii) optimal beamforming and power allocation. For optimal port selection, (7) can be simplified as

$$\max_{\boldsymbol{A}} R\left(\boldsymbol{A}, \boldsymbol{W}, \boldsymbol{P}\right) \quad \text{s.t.} \quad (7b), (7c), (7d). \qquad (8)$$

However, it is still challenging to solve (8) since the objective function cannot be directly evaluated. To overcome this problem, we exploit the fact that $R\left(\boldsymbol{A}, \boldsymbol{W}, \boldsymbol{P}\right)$ strongly depends on $\det(\bar{\boldsymbol{H}} \bar{\boldsymbol{H}}^H)$ in the high SNR regime [28]. Thus, (8) can be relaxed as

$$\max_{\boldsymbol{A}} \det(\bar{\boldsymbol{H}} \bar{\boldsymbol{H}}^H) \quad \text{s.t.} \quad (7b), (7c), (7d), \qquad (9)$$

[5]As will be shown later in this paper, $N_s, \forall s$ can be represented by a finite constant even in cases where $N_s \to \infty$.

which is unfortunately still an NP-hard problem [29].[6] However, we can obtain a suboptimal solution by using the strong rank-revealing QR (RRQR) factorization [30].

Specifically, by applying QR factorization with pivoted column on $\boldsymbol{H}^H$, we have

$$\boldsymbol{H}^H \boldsymbol{\Pi} = \boldsymbol{Q} \boldsymbol{R}, \qquad (10)$$

where $\boldsymbol{\Pi}$ is a permutation matrix, $\boldsymbol{Q}$ is an orthogonal matrix and $\boldsymbol{R}$ is an upper triangular matrix where the absolute of leading entries in $\boldsymbol{R}$ are decreasing in values. The upper triangular matrix $\boldsymbol{R}$ can be rewritten as

$$\boldsymbol{R} = [\boldsymbol{R}_1 \; \boldsymbol{R}_2] = \begin{bmatrix} \boldsymbol{S}_1 & \boldsymbol{S}_2 \\ \boldsymbol{0} & \boldsymbol{S}_3 \end{bmatrix}, \qquad (11)$$

where $\boldsymbol{R_1} = [\boldsymbol{S}_1 \; \boldsymbol{0}]^T$ and $\boldsymbol{R_2} = [\boldsymbol{S}_2 \; \boldsymbol{S}_3]^T$. Substituting (11) into (10), we obtain

$$\left[\boldsymbol{H}^H \boldsymbol{\Pi}_a \; \boldsymbol{H}^H \boldsymbol{\Pi}_i\right] = \left[\boldsymbol{H}_a^H \; \boldsymbol{H}_i^H\right] = [\boldsymbol{Q}\boldsymbol{R}_1 \; \boldsymbol{Q}\boldsymbol{R}_2], \quad (12)$$

in which $\boldsymbol{\Pi} = [\boldsymbol{\Pi}_a \; \boldsymbol{\Pi}_i]$. In (12), the left hand side and right hand side of (10) are separated into two blocks and thus we can interpret $\boldsymbol{H}_a^H$ and $\boldsymbol{H}_i^H$ as the MIMO-FAS channels of active and inactive ports, respectively. Since the singular values of $\boldsymbol{H}^H$ and $\boldsymbol{R}$ remain the same, it is clear that (12) provides the following properties

$$\prod_{m=1}^{N_{\min}} \sigma_m \left(\boldsymbol{H}^H\right) = \prod_{m=1}^{n_s} \sigma_m \left(\boldsymbol{H}_a^H\right) \prod_{m=n_s+1}^{N_{\min}} \sigma_m \left(\boldsymbol{H}_i^H\right)$$

$$= \prod_{m=1}^{n_s} \sigma_m \left(\boldsymbol{R}_1\right) \prod_{m=n_s+1}^{N_{\min}} \sigma_m \left(\boldsymbol{R}_2\right), \quad (13)$$

where $N_{\min} = \min \{N_{rx}, N_{tx}\}$ and $\sigma_m \left(\cdot\right)$ denotes the m-th singular value of the matrix argument.

In alignment with (9), our objective here is to maximize $\prod_{m=1}^{n_s} \sigma_m \left(\boldsymbol{H}_a^H\right)$ in (13) by permuting the k-th column of $\boldsymbol{H}_a^H$ and the l-th column of $\boldsymbol{H}_i^H$. To facilitate this objective, we employ the matrix $\boldsymbol{\Omega}$ where the (k, l)-th entry of $\boldsymbol{\Omega}$ is

$$\Omega_{k,l} = \sqrt{\left|\boldsymbol{S}_1^\dagger \boldsymbol{S}_2\right|_{k,l}^2 + \|\boldsymbol{s}_{3,l}\|_2^2 + \left\|\boldsymbol{s}_{1,k}^{\dagger,T}\right\|_2^2}, \qquad (14)$$

where $|\boldsymbol{S}|_{k,l}$ gives the absolute value of the (k, l)-th entry of $\boldsymbol{S}$, $\boldsymbol{s}_{s,l}$ is the l-th column of $\boldsymbol{S}_s$ and $\boldsymbol{s}_{s,k}^{\dagger,T}$ is the k-th row of $\boldsymbol{S}_s^\dagger$. Furthermore, let us denote $\boldsymbol{H}_{a,k,l}^H$ (or $\boldsymbol{\Pi}_{a,k,l}$) is the new matrix where the k-th column of $\boldsymbol{H}_a^H$ (or $\boldsymbol{\Pi}_a$) and the l-th column of $\boldsymbol{H}_i^H$ (or $\boldsymbol{\Pi}_i$) are permuted.

Conventionally, it is necessary to permute all the (k, l) combinations and find the maximum $\prod_{m=1}^{n_s} \sigma_m \left(\boldsymbol{H}_{a,k,l}^H\right)$ in the presence of spatial correlation. Nevertheless, using (14), we can determine the increase or decrease of $\prod_{m=1}^{n_s} \sigma_m \left(\boldsymbol{H}_{a,k,l}^H\right)$ over $\prod_{m=1}^{n_s} \sigma_m \left(\boldsymbol{H}_a^H\right)$ before permuting them. Hence, we can

[6]The relaxation is done because $R\left(\boldsymbol{A}, \boldsymbol{W}, \boldsymbol{P}\right) \approx \log \det(\bar{\boldsymbol{H}} \boldsymbol{K} \bar{\boldsymbol{H}}^H)$ at high SNR and the rate of using equal power allocation approaches to that of waterfilling power allocation as SNR increases [37]. For other SNR regimes, solving (7) with low complexity remains open. Nevertheless, we can obtain an efficient solution at low SNR by activating n_{rx}/n_{tx} ports where the row/column-norm of $\boldsymbol{H}$ are the largest and they are separated by at least c_{rx}/c_{tx} distance. We refer this scheme as the greedy selection.

Algorithm 1 Pseudocode of QR MIMO-FAS

1: Compute (10) via QR factorization with pivoted column
2: Compute $\mathbf{\Omega}$ using (14)
3: **While** $\Omega_{k,l} > 1$
4: Permute the k-th column of $\boldsymbol{H}_a^H/\boldsymbol{\Pi}_a$ and the l-th column of $\boldsymbol{H}_i^H/\boldsymbol{\Pi}_i$ with the largest $\Omega_{k,l} > 1$
5: Update $\boldsymbol{H}^H = \boldsymbol{H}_{a,k,l}^H$ and $\boldsymbol{\Pi} = \boldsymbol{\Pi}_{a,k,l}$
6: Perform QR factorization using $\boldsymbol{\Pi}$ and return to Step 2
7: **end**
8: Set $\boldsymbol{A}_r^* = \boldsymbol{\Pi}_a^T$
9: Repeat Steps 1–7 by replacing $\boldsymbol{H}^H$ with $\boldsymbol{A}_r^*\boldsymbol{H}$
10: Set $\boldsymbol{A}_r^* = \boldsymbol{\Pi}_a^T$
11: Compute SVD on $\boldsymbol{A}_r^*\boldsymbol{H}\boldsymbol{A}_t^*$ to obtain $\boldsymbol{W}^*$
12: Use bisection to obtain $\boldsymbol{P}^*$

---

directly permute the k-th column of $\boldsymbol{H}_a^H$ (and $\boldsymbol{\Pi}_a$) and the l-th column of $\boldsymbol{H}_i^H$ (and $\boldsymbol{\Pi}_i$) and then update $\boldsymbol{H}^H = \boldsymbol{H}_{a,k,l}^H$ (and $\boldsymbol{\Pi} = \boldsymbol{\Pi}_{a,k,l}$) if $\Omega_{k,l} > 1$. In this paper, we permute the columns based on the largest $\Omega_{k,l}$ which yields a suboptimal solution. Furthermore, we perform QR factorization to obtain the expression in (10) with the existing $\boldsymbol{\Pi}$. These steps can be repeated until $\Omega_{k,l} \leq 1 \ \forall k, l$. Using strong RRQR factorization, we can obtain $\boldsymbol{H}_a^H$ with the maximum $\prod_{m=1}^{n_s} \sigma_m\left(\boldsymbol{H}_a^H\right)$ where $\boldsymbol{A}_{rx}^* = \boldsymbol{\Pi}_a^T$. Reapplying strong RRQR factorization on $\boldsymbol{A}_{rx}^*\boldsymbol{H}$, we can also obtain $\boldsymbol{A}_{tx}^*$ where $\boldsymbol{A}_{tx}^* = \boldsymbol{\Pi}_a$.

Given $\boldsymbol{A}^*$, (7) reduces to the optimal beamforming and power allocation problem which can be formulated as

$$\max_{\boldsymbol{W},\boldsymbol{P}} R\left(\boldsymbol{W}, \boldsymbol{P}|\boldsymbol{A}^*\right) \quad \text{s.t.} \quad (7e), (7f). \tag{15}$$

Interestingly, (15) can be easily solved via SVD and waterfilling power allocation [27]. In particular, the solution to (15) is $\boldsymbol{W}_r^* = \bar{\boldsymbol{M}}^H$ and $\boldsymbol{W}_t^* = \bar{\boldsymbol{N}}$ where $\bar{\boldsymbol{H}} = \bar{\boldsymbol{M}}\bar{\boldsymbol{\Sigma}}\bar{\boldsymbol{N}}^H$, $\bar{\boldsymbol{M}}$ is the left singular matrix of $\bar{\boldsymbol{H}}$, $\bar{\boldsymbol{N}}$ is the right singular matrix of $\bar{\boldsymbol{H}}$, $\bar{\boldsymbol{\Sigma}} = \text{diag}\left(\bar{\Sigma}_1, \ldots, \bar{\Sigma}_{n_{\min}}\right)$ denotes the diagonal matrix whose l-th entry is the l-th singular value of $\bar{\boldsymbol{H}}$, $\bar{\Sigma}_1 \geq \cdots \geq \bar{\Sigma}_{n_{\min}}$ and $n_{\min} = \min\{n_{tx}, n_{rx}\}$. In addition, $\boldsymbol{P}^* = \text{diag}\left(p_1^*, \ldots, p_{n_{\min}}^*\right)$, $p_l^* = \left[\mu - \frac{1}{\bar{\Sigma}_l^2}\right]_0^+$, and $\text{SNR} = \sum p_l^*$.[7] Thus, the optimal input covariance is $\boldsymbol{K}^* = \boldsymbol{W}_{tx}^*\boldsymbol{P}^*\boldsymbol{W}_{tx}^{*H}$. Using the above methods, the rate of the QR MIMO-FAS for a given SNR can be expressed as

$$R_{\text{QR}}\left(\text{SNR}\right) = \sum_{l=1}^{n_{\min}} \log\left(1 + p_l^*\bar{\Sigma}_l^2\right), \tag{16}$$

where (16) helps analyze the optimal DMT of MIMO-FAS.

The pseudocode of the proposed scheme is presented in Algorithm 1. Let us denote $N_{\max} = \max\{N_{tx}, N_{rx}\}$ and $n_{\max} = \max\{n_{tx}, n_{rx}\}$. The worst computational cost of Step 1 is $\frac{4}{3}n_{\max}^3 - 4N_{\max}n_{\max}^2 + 4N_{\max}^2 n_{\max}$ flops [30]. Steps 2–7 require $(1+t_i)\left[\left(\frac{2}{3}n_{\max}^3 N_{\max}^2 + 2n_{\max}^2 N_{\max}^3 + 2N_{\max}^3\right)\right]$ flops [31], where t_i is a finite number of permutations and it

is usually small due to Step 1 [28]. Step 9 has the same total computational cost as Steps 1–7, which is also finite. In addition, Steps 11 and 12 require $21n_{\max}^3$ and $\log\left(\frac{\mu_{\max}}{\epsilon_0}\right)n_{\max}$ flops, respectively, where $\mu_{\max}$ is the interval for searching μ and ϵ_0 is the tolerance for bisection method. Summing up the computational costs, the proposed scheme has a polynomial time complexity of $\mathcal{O}\left(n_{\max}^3 N_{\max}^3\right)$. Compared to the global optimal solution, the proposed scheme significantly reduces the time complexity.

IV. OPTIMAL DMT

In this section, we analyze the optimal DMT of MIMO-FAS. As defined in [24], a MIMO scheme is said to achieve a multiplexing gain of r and a diversity gain of d if

$$\lim_{\text{SNR}\to\infty} \frac{R_{\text{sys}}\left(\text{SNR}\right)}{\log\text{SNR}} = r, \tag{17}$$

and the outage probability satisfies[8]

$$\lim_{\text{SNR}\to\infty} \frac{\log\left(P_{\text{sys}}^{\text{out}}\left(\text{SNR}, r\right)\right)}{\log\text{SNR}} = -d\left(r\right), \tag{18}$$

in which $R_{\text{sys}}\left(\text{SNR}\right)$ and $P_{\text{sys}}^{\text{out}}\left(\text{SNR}, r\right)$ are, respectively, the rate and outage probability of the system. Similar to [24], we use the symbol $\doteq$ to denote exponential equality. In particular, $f\left(\text{SNR}\right) \doteq \text{SNR}^{-d}$ if

$$\lim_{\text{SNR}\to\infty} \frac{\log\left(f\left(\text{SNR}\right)\right)}{\log\text{SNR}} = -d. \tag{19}$$

To obtain the optimal DMT of MIMO-FAS, we present the following lemmas.

Lemma 1. *Given a 2D space with an area of W_s where both $W_1^s \gg 0$ and $W_2^s \gg 0$, $\boldsymbol{J}_s$ in (2) can be represented by $\boldsymbol{J}_{\text{red}}^s$, i.e., a full rank symmetric $N_s' \times N_s'$ finite-size matrix even if $N_s \to \infty$.*

Proof: For a positive W_s, consider (2) where $N_s \to \infty$. Without loss of generality, we focus on two neighboring ports: the (n_1^s, n_2^s)-th and $(\tilde{n}_1^s, \tilde{n}_2^s)$-th port. In cases where $N_1^s \to \infty$, we analyze $(\tilde{n}_1^s, \tilde{n}_2^s) = (n_1^s \pm 1, n_2^s)$. The spatial correlation between the (n_1^s, n_2^s)-th and $(\tilde{n}_1^s, \tilde{n}_2^s)$-th port is given by

$$J_{\left(n_1^s, n_2^s\right),\left(\tilde{n}_1^s, n_2^s\right)}^s = \lim_{N_1^s \to \infty} j_0\left(\frac{2\pi}{N_1^s - 1}W_1^s\right) = 1, \tag{20}$$

since $\lim_{N_1^s \to \infty} \frac{1}{N_1^s - 1} = 0$. In other words, the spatial correlation of the $\tilde{n}_1^s$-th port is identical to that of the n_1^s-th port in the limit. For ease of exposition, let us refer to the spatial correlation of a port as an entry.

For $n_2^s = \{1, \ldots, N_2^s\}$, we can remove the identical entries (e.g., $\tilde{n}_1^s$ for $\exists n_1^s$) and obtain $\bar{N}_1^s$ distinct entries. Next, let us denote the $(\dot{n}_1^s, n_2^s)$-th port as the farthest port away from the (n_1^s, n_2^s)-th port. Since $W_1^s \gg 0$, it is clear that $J_{\left(n_1^s, n_2^s\right),\left(\dot{n}_1^s, n_2^s\right)}^s = j_0\left(2\pi\dot{c}\right)$ where $\dot{c} \gg 0$ is the distance

---

[7]Note that it is possible to employ equal power allocation at high SNR. In fact, our analysis leverages this assumption for tractability. Nevertheless, we will consider waterfilling power allocation here since it is optimal regardless of the SNR. In addition, it would be useful later to make a fair comparison between different benchmarking schemes.

[8]Here, we use the fact that the error probability can be arbitrarily close to the outage probability [32], [33].

between the $(\dot{n}_1^s, n_2^s)$-th and (n_1^s, n_2^s)-th ports. By intermediate value theorem, we can conclude there is an ε such that

$$\varepsilon = \inf \left\{ e \left| J_{(n_1^s, n_2^s),(n_1^s \pm e, n_2^s)}^s \neq 1, \begin{array}{l} e \in \mathbb{N}, \\ 0 < e \leq N_1^s - 1 \end{array} \right. \right\}. \tag{21}$$

Note that one cannot make any assumption on e and ε except their existence. Let us define $c_1^s \triangleq \frac{\varepsilon}{N_1^s - 1} W_1^s$ as the minimal distance required for the spatial correlation between the (n_1^s, n_2^s)-th and $(n_1^s \pm e, n_2^s)$-th ports to be completely distinct. Then we can verify that $\bar{N}_1^s$ is finite since $W_1^s \geq \bar{N}_1^s c_1^s > 0$. Let us write the $\bar{N}_1^s$ distinct entries as a vector $\boldsymbol{v}_{n_2^s}$ for each $n_2^s \in \{1, \ldots, N_2^s\}$. If these vectors are linearly dependent, then we can similarly remove the dependent vectors and obtain $\bar{N}_2$ independent vectors. As a result, we can rewrite $\boldsymbol{J}_s$ as a symmetric $\bar{N}_s \times \bar{N}_s$ finite-size matrix with distinct entries where $\bar{N}_s = \bar{N}_1^s \bar{N}_2^s$.

Using a similar argument, we see that $\boldsymbol{J}_s$ can be represented by an $\bar{N}_s \times \bar{N}_s$ finite-size matrix if $N_2^s \to \infty$. Combining the two cases, it is straightforward to see that $\boldsymbol{J}_s$ can be rewritten as a symmetric $\bar{N}_s \times \bar{N}_s$ matrix as $N_1^s \to \infty$ and $N_2^s \to \infty$ since both $W_1^s \gg 0$ and $W_2^s \gg 0$, and we have (21) and

$$\varepsilon_2 = \inf \left\{ e \left| J_{(n_1^s, n_2^s),(n_1^s, n_2^s \pm e)}^s \neq 1, \begin{array}{l} e \in \mathbb{N}, \\ 0 < e \leq N_2^s - 1 \end{array} \right. \right\}. \tag{22}$$

From the above, it is clear that we can use the same argument to show that $\boldsymbol{J}_s$ can be rewritten as a symmetric $\bar{N}_s \times \bar{N}_s$ matrix if N_1^s / N_2^s is finite since we can always remove the entries where their vertical/horizontal distances between the adjacent ports are less than c_1^s / c_2^s.

Let us denote N_s' as the full rank of the symmetric $\bar{N}_s \times \bar{N}_s$ matrix where $N_s' \leq \bar{N}_s$. Then we can further reduce the symmetric $\bar{N}_s \times \bar{N}_s$ matrix to a full rank symmetric $N_s' \times N_s'$ submatrix $\boldsymbol{J}_{\text{red}}^s$ by removing the $(\bar{N}_s - N_s')$ dependent rows and columns. Thus, $\boldsymbol{J}_s$ can always be represented by $\boldsymbol{J}_{\text{red}}^s$, i.e., a full rank symmetric $N_s' \times N_s'$ finite-size matrix. In other words, it suffices to consider $\boldsymbol{J}_{\text{red}}^s$ instead of $\boldsymbol{J}_s$ since some rows/columns of $\boldsymbol{J}_s$ are identical or a linear combination of the others. A more general result is given in Appendix II. ∎

Lemma 2. *If $\boldsymbol{J}_{tx}$ and $\boldsymbol{J}_{rx}$ are full rank, the optimal DMT of any MIMO system with channel $\boldsymbol{H}$ is the same as that of a system with channel $\boldsymbol{G}$.*

Proof: See [34]. ∎

Lemma 3. *The optimal DMT of using only $n_{rx} \times n_{tx}$ channels from the MIMO channel $\boldsymbol{G}$, where $n_{tx} \leq N_{tx}$ and $n_{rx} \leq N_{rx}$, is a piecewise linear function connecting the points $(n_{\min}, 0)$ and*

$$\{r, (N_{rx} - r)(N_{tx} - r)\}, \quad r = 0, \ldots, N, \tag{23}$$

where

$$N = \arg \min_{\substack{\eta \in \mathbb{Z} \\ 0 \leq \eta \leq n_{\min} - 1}} \frac{(N_{rx} - \eta)(N_{tx} - \eta)}{n_{\min} - \eta}. \tag{24}$$

Proof: See [35]. ∎

Corollary 1. *If the antennas are placed based on a grid structure with at least half a wavelength apart and the transmit/receive spatial correlation matrices are full rank, then*

the optimal DMT of $n_{rx} \times n_{tx}$ MIMO antenna selection is a piecewise linear function connecting the points $(n_{\min}, 0)$ and

$$\{r, (w_{rx} - r)(w_{tx} - r)\}, \quad r = 0, \ldots, N_{as}, \tag{25}$$

where

$$N_{as} = \arg \min_{\substack{\eta \in \mathbb{Z} \\ 0 \leq \eta \leq n_{\min} - 1}} \frac{(w_{rx} - \eta)(w_{tx} - \eta)}{n_{\min} - \eta}. \tag{26}$$

Proof: Given a fixed W_s^1 and W_s^2, there can be at most $w_s = \left(\left\lfloor \frac{W_s^1}{0.5} \right\rfloor + 1 \right) \left(\left\lfloor \frac{W_s^2}{0.5} \right\rfloor + 1 \right)$ antennas at side s. Using Lemma 2 and Lemma 3, we obtain (25) and (26). ∎

Using the above lemmas, we can now obtain the outer bound of the DMT of MIMO-FAS.

Theorem 1. *For finite W_{rx} and W_{tx}, the outer bound of the DMT of MIMO-FAS is a piecewise linear function connecting the points $(n_{\min}, 0)$ and*

$$\left\{ r, \left(N_{rx}' - r \right) \left(N_{tx}' - r \right) \right\}, \quad r = 0, \ldots, N', \tag{27}$$

where

$$N' = \arg \min_{\substack{\eta \in \mathbb{Z} \\ 0 \leq \eta \leq n_{\min} - 1}} \frac{\left(N_{rx}' - \eta \right) \left(N_{tx}' - \eta \right)}{n_{\min} - \eta}. \tag{28}$$

Proof: By using SVD, we can decompose $\boldsymbol{H} = \boldsymbol{M} \boldsymbol{\Sigma} \boldsymbol{N}$ where $\boldsymbol{M}$ is the left singular matrix of $\boldsymbol{H}$, $\boldsymbol{N}$ is the right singular matrix of $\boldsymbol{H}$, $\boldsymbol{\Sigma} = \text{diag}\left(\Sigma_1, \ldots, \Sigma_{N_{\min}} \right)$ is a diagonal matrix whose l-th entry is the singular value of $\boldsymbol{H}$ and $\Sigma_1 \geq \cdots \geq \Sigma_{N_{\min}}$. According to the Cauchy's Interlacing theorem [36], it follows that $\Sigma_1 \geq \bar{\Sigma}_1 \geq \cdots \geq \bar{\Sigma}_{n_{\min}} \geq \Sigma_{n_{\min}} \geq \cdots \geq \Sigma_{N_{\min}}$. Therefore, the rate of MIMO-FAS can be upper bounded by

$$R(\text{SNR}) = \sum_{l=1}^{n_{\min}} \log \left(1 + \tilde{p}_l^* \Sigma_l^2 \right), \tag{29}$$

where $\tilde{p}_l^* = \left[\mu - \frac{1}{\Sigma_l^2} \right]_0^+$ and $\text{SNR} = \sum \tilde{p}_l^*$. At high SNR, (29) can be simplified as

$$R(\text{SNR}) = \sum_{l=1}^{n_{\min}} \log \left(1 + \frac{\text{SNR}}{n_{\min}} \Sigma_l^2 \right), \tag{30}$$

since the rate of using equal power allocation approaches to that of waterfilling power allocation as SNR increases [37]. Consequently, the outage probability of MIMO-FAS can be lower bounded by

$$P_{\text{out}}(\text{SNR}, r) = \mathbb{P} \left\{ R(\text{SNR}) < r \log \text{SNR} \right\}. \tag{31}$$

At high SNR, the outage probability is rewritten as [24]

$$P_{\text{out}}(\text{SNR}, r) = \mathbb{P} \left\{ \sum_{l=1}^{n_{\min}} \log \left(1 + \text{SNR} \Sigma_l^2 \right) < r \log \text{SNR} \right\}, \tag{32}$$

since

$$
\begin{aligned}
&\lim_{\mathrm{SNR}\to\infty} \frac{\log\left(\mathbb{P}\left\{\sum_{l=1}^{n_{\min}}\log\left(1+\frac{\mathrm{SNR}}{n_{\min}}\Sigma_l^2\right)<r\log\mathrm{SNR}\right\}\right)}{\log\mathrm{SNR}}\\
&=\lim_{\mathrm{SNR}\to\infty} \frac{\log\left(\mathbb{P}\left\{\sum_{l=1}^{n_{\min}}\log\left(1+\frac{\mathrm{SNR}}{n_{\min}}\Sigma_l^2\right)<r\log\mathrm{SNR}\right\}\right)}{\log\frac{\mathrm{SNR}}{n_{\min}}}\\
&=\lim_{\mathrm{SNR}\to\infty} \frac{\log\left(\mathbb{P}\left\{\sum_{l=1}^{n_{\min}}\log\left(1+\mathrm{SNR}\Sigma_l^2\right)<r\log\mathrm{SNR}\right\}\right)}{\log\mathrm{SNR}}.
\end{aligned}
\tag{33}
$$

Using (19), we can obtain the outer bound on the diversity gain for a fixed multiplexing gain r as

$$
P_{\mathrm{out}}\left(\mathrm{SNR},r\right)\doteq\mathbb{P}\left\{\sum_{l=1}^{n_{\min}}\log\left(1+\mathrm{SNR}\Sigma_l^2\right)<r\log\mathrm{SNR}\right\}.
\tag{34}
$$

According to [38], the joint probability density function (PDF) of $\boldsymbol{\Sigma}^2$ is given by

$$
\begin{aligned}
f\left(\boldsymbol{\Sigma}^2\right)=\sum_{\boldsymbol{q}}&\frac{(-1)^{\frac{N_{\min}(N_{\min}-1)}{2}}\mathcal{A}}{N_{\min}!\triangle\left(\boldsymbol{q}\right)}\triangle\left(\boldsymbol{\Sigma}^2\right)\times\\
&\det\left(\boldsymbol{\Sigma}_k^{2(q_l+N_{\max}-N_{\min})}\right),
\end{aligned}
\tag{35}
$$

where $\boldsymbol{q}=[q_1,\ldots,q_{N_{\max}}]^T$, $N_{\min}=\min\{N_{tx},N_{rx}\}$,

$$
\begin{aligned}
\mathcal{A}=&\frac{\prod_{k=1}^{N_{\min}}\lambda_k^s\prod_{l=1}^{N_{\max}}\lambda_l^{s'}\det\left((-\lambda_k^s)^{q_l}\right)}{\triangle\left(\boldsymbol{\lambda}^s\right)\triangle\left(\boldsymbol{\lambda}^{s'}\right)}\times\\
&\frac{\det\left(\left(\lambda_k^{s'}\right)^{q_l+N_{\max}-N_{\min}}\Big|_{k=1}^{N_{\min}},\left(\lambda_i^{s'}\right)^{N_{\max}-k}\Big|_{k=N_{\min}+1}^{N_{\max}}\right)}{\prod_{l=1}^{N_{\min}}(q_l+N_{\max}-N_{\min})!},
\end{aligned}
\tag{36}
$$

where

$$
\begin{cases}
s=\{s|N_s=\min\{N_{tx},N_{rx}\}\},\\
s'=\{s'|N_{s'}=\max\{N_{tx},N_{rx}\}\},\\
\boldsymbol{\lambda}^s=\left[\lambda_1^s,\ldots,\lambda_{N_s}^s\right]^T,
\end{cases}
\tag{37}
$$

$\triangle\left(\boldsymbol{\lambda}^s\right)$ denotes the Vandermonde determinant of vector $\boldsymbol{\lambda}^s$, $\det\left(f\left(k,l\right)\right)$ is the determinant of a matrix with the (k,l)-th entry given by the function $f\left(k,l\right)$ and $q_l=b_l+N_{\max}-l$. In addition, $\boldsymbol{b}=[b_1,\ldots,b_{N_{\max}}]^T$ is the irreducible representation of unitary group such that $b_1\geq\cdots\geq b_{N_{\max}}\geq 0$ are integers.

Conventionally, we can analyze the outer bound by simplifying the joint PDF of $\boldsymbol{\Sigma}^2$ and then analyzing the exponents of Σ_l. Nevertheless, it is found that no simplification can be made to keep the exponents of Σ_l tractable when the rows and columns of $\boldsymbol{H}$ are fully correlated [39]. To alleviate this problem, we employ Lemma 1, Lemma 2, and Lemma 3.

Specifically, according to [40], the PDF of $\boldsymbol{H}$ can be obtained by removing the dependent entries and the PDF of the singular values of $\boldsymbol{H}$ can be obtained via coordinate changes [41]. Using Lemma 1, we know that $\boldsymbol{J}_s$ can be represented by a full rank symmetric finite-size matrix, i.e, $\boldsymbol{J}_{\mathrm{red}}^s\in\mathbb{R}^{N_s'\times N_s'}$ and $\mathrm{rank}\left(\boldsymbol{J}_{\mathrm{red}}^s\right)=N_s'$. It follows that $\boldsymbol{H}$ and $\boldsymbol{G}$ in (3) can be rewritten as $N_{rx}'\times N_{tx}'$ matrices with the same PDFs. From Lemma 2, it is known that the DMT

of any MIMO system with channel $\boldsymbol{H}\in\mathbb{C}^{N_{rx}'\times N_{tx}'}$ is the same as that of a system with channel $\boldsymbol{G}\in\mathbb{C}^{N_{rx}'\times N_{tx}'}$. Since $\boldsymbol{G}$ is an independent and identically distributed (i.i.d.) circularly symmetric complex Gaussian matrix, it follows that $\mathrm{rank}\left(\boldsymbol{G}\right)=N_{\min}'=\min\{N_{rx}',N_{tx}'\}$ with probability one. Using Lemma 3, we can conclude that the outer bound of the DMT of MIMO-FAS is a piecewise linear function connecting the points as given in (27) and (28). ∎

Using Theorem 1, we can now derive the optimal DMT of MIMO-FAS by considering its outer bound and inner bound. Specifically, the DMT of QR MIMO-FAS can be regarded as the inner bound of the DMT of MIMO-FAS.

Theorem 2. *The DMT of QR MIMO-FAS is equivalent to the outer bound of the DMT of MIMO-FAS, and thus it is also the optimal DMT of MIMO-FAS.*

Proof: At high SNR, (16) can be simplified as

$$
R_{\mathrm{QR}}\left(\mathrm{SNR}\right)=\sum_{l=1}^{n_{\min}}\log\left(1+\frac{\mathrm{SNR}}{n_{tx}}\bar{\Sigma}_l^2\right)
\tag{38}
$$

since the rate of using equal power allocation approaches to that of waterfilling power allocation as SNR increases [37]. Consequently, the outage probability is characterized by

$$
P_{\mathrm{QR}}^{\mathrm{out}}\left(\mathrm{SNR},r\right)=\mathbb{P}\left\{R_{\mathrm{QR}}\left(\mathrm{SNR}\right)<r\log\mathrm{SNR}\right\}.
\tag{39}
$$

At high SNR, the difference between (30) and (38) is

$$
R\left(\mathrm{SNR}\right)-R_{\mathrm{QR}}\left(\mathrm{SNR}\right)\approx\sum_{l=1}^{n_{\min}}\log\left(\frac{n_{tx}\Sigma_l^2}{n_{\min}\bar{\Sigma}_l^2}\right)=c_0,
\tag{40}
$$

which is a constant.[9] As $\lim_{c\to\infty}\log\left(\frac{1+c}{c}\right)=0$, the approximation of (40) is tight as $\mathrm{SNR}\to\infty$. As such, we have

$$
\begin{aligned}
\lim_{\mathrm{SNR}\to\infty}\frac{R_{\mathrm{QR}}\left(\mathrm{SNR}\right)}{\log\mathrm{SNR}}&=\lim_{\mathrm{SNR}\to\infty}\frac{R\left(\mathrm{SNR}\right)-c_0}{\log\mathrm{SNR}}\\
&=\lim_{\mathrm{SNR}\to\infty}\frac{R\left(\mathrm{SNR}\right)}{\log\mathrm{SNR}},
\end{aligned}
\tag{41}
$$

and

$$
\begin{aligned}
&\lim_{\mathrm{SNR}\to\infty}\frac{\log\left(P_{\mathrm{QR}}^{\mathrm{out}}\left(\mathrm{SNR},r\right)\right)}{\log\mathrm{SNR}}\\
&=\lim_{\mathrm{SNR}\to\infty}\frac{\log\left(\mathbb{P}\left\{R\left(\mathrm{SNR}\right)<r\log\mathrm{SNR}+c_0\right\}\right)}{\log\mathrm{SNR}}\\
&=\lim_{\mathrm{SNR}\to\infty}\frac{\log\left(\mathbb{P}\left\{R\left(\mathrm{SNR}\right)<r\log\mathrm{SNR}\right\}\right)}{\log\mathrm{SNR}}\\
&=\lim_{\mathrm{SNR}\to\infty}\frac{\log\left(P_{\mathrm{out}}\left(\mathrm{SNR},r\right)\right)}{\log\mathrm{SNR}}.
\end{aligned}
\tag{42}
$$

Thus, the DMT of QR MIMO-FAS is equivalent to the outer bound, and also the optimal DMT of MIMO-FAS. ∎

It is challenging to explicitly obtain N_s' because $\boldsymbol{J}_s$ might be near to being singular. It is also unclear how $\boldsymbol{J}_s$ can be reduced to/reconstructed from $\boldsymbol{J}_{\mathrm{red}}^s$. To address these issues, we propose methods to reliably estimate N_s', and to linearly transform $\boldsymbol{J}_s$ to $\boldsymbol{J}_{\mathrm{red}}^s$ and vice versa with a proof of certificates. These methods are based on the following theorems.

---

[9]Note that a constant gap amounts to a finite scaling of SNR. This implies that $R\left(\mathrm{SNR}\right)=R_{\mathrm{QR}}\left(\mathrm{SNR}+\gamma\right)$ for some $\gamma>0$.

This article has been accepted for publication in IEEE Transactions on Wireless Communications. This is the author's version which has not been fully edited and content may change prior to final publication. Citation information: DOI 10.1109/TWC.2023.3327063

9

Table II: Estimation of N'_s for different W_s in terms of λ^2, where $\xi = 10^{-3}$, $N_s = 100$, $N_1^s = N_2^s$, and $W_1^s = W_2^s$.

W_s	0.5×0.5	1×1	1.5×1.5	2×2	2.5×2.5	3×3
N'_s	13	23	34	48	60	73
E	0.001	0.002	0.003	0.002	0.005	0.005

[‡] Note that the figures regarding the diversity order of MIMO-FAS described in [25] were based on an earlier version of this paper considering the spatial correlation in 2D environments only. The correct diversity orders for MIMO-FAS in 3D environments should be referred to this table. For example, for MIMO-FAS with $0.5\lambda \times 0.5\lambda$ FAS at both ends, the diversity order is $13 \times 13 = 169$ which is much higher than originally reported.

Theorem 3. *Since $\boldsymbol{J}_s$ can be well-approximated by $\hat{\boldsymbol{J}}_s$ where $\hat{\boldsymbol{J}}_s = \boldsymbol{U}_s \hat{\boldsymbol{\Lambda}} \boldsymbol{U}_s^H$ and $\hat{\boldsymbol{\Lambda}} = \mathrm{diag}(\lambda_1^s, \ldots, \lambda_{N'_s}^s, 0, \ldots, 0)$, the rank of $\boldsymbol{J}_s$ can be estimated as N'_s.*

Proof: Define an arbitrarily small $\xi > 0$ as the threshold where the numerical values of the eigenvalues are negligible. According to [42], $\boldsymbol{J}_s$ can be regularized by $\hat{\boldsymbol{J}}_s$, where $\hat{\boldsymbol{J}}_s = \boldsymbol{U}_s \hat{\boldsymbol{\Lambda}} \boldsymbol{U}_s^H$, $\hat{\boldsymbol{\Lambda}} = \mathrm{diag}(\lambda_1^s, \ldots, \lambda_{N'}^s, 0, \ldots, 0)$ and $\lambda_l^s < \xi$, $l \in \{N'_s + 1, \ldots, N_s\}$. The Frobenius norm between $\boldsymbol{J}_s$ and $\hat{\boldsymbol{J}}_s$ is given by

$$E = \|\boldsymbol{J}_s - \hat{\boldsymbol{J}}_s\|_F = \sum_{l=N'_s+1}^{N_s} \lambda_l^s, \qquad (43)$$

which can be upper bounded by $(N_s - N'_s)\xi$. In practice, we have $\lambda_1^s \gg \lambda_{N'_s+1}^s > \ldots > \lambda_{N_s}^s$ and thus (43) is usually very small. Therefore, the rank of $\boldsymbol{J}_s$ can be estimated as N'_s. ∎

Theorem 4. *For arbitrary $N_s = N_1^s \times N_2^s$ and a finite $W_s = W_1^s \times W_2^s$, $\boldsymbol{J}_s$ in (2) can be reduced to $\boldsymbol{J}_{\mathrm{red}}^s$ using the set $\mathcal{V}_s = \{\boldsymbol{v}_l^s | \boldsymbol{J}_s^{(l)} \tilde{\boldsymbol{v}}_l^s = \boldsymbol{0}, l = N'_s + 1, \ldots, N_s\}$ where $\tilde{\boldsymbol{v}}_l^s = [\boldsymbol{v}_l^s \ -1]^T$. Conversely, $\boldsymbol{J}_s$ in (2) can be reconstructed from $\boldsymbol{J}_{\mathrm{red}}^s$ with the set $\mathcal{V}_s$.*

Proof: Let us introduce a vector $\tilde{\boldsymbol{v}}_l^s = [\boldsymbol{v}_l^s \ -1]^T$ where $\boldsymbol{v}_l^s \in \mathbb{R}^l$ and $\boldsymbol{v}_l^s \neq \boldsymbol{0}$. In addition, let us denote

$$\boldsymbol{J}_s^{(l)} = \begin{bmatrix} \boldsymbol{J}_{\mathrm{sub}}^{(l-1)} & \boldsymbol{j}_l \\ \boldsymbol{j}_l^T & j_{l,l} \end{bmatrix}. \qquad (44)$$

Note that $\boldsymbol{J}_s = \boldsymbol{J}_s^{(N_s)}$ and $\boldsymbol{J}_{\mathrm{red}}^s = \boldsymbol{J}_s^{(N'_s)}$. If $N'_s = N_s$, then $\mathcal{V}_s$ is an empty set and $\boldsymbol{J}_s = \boldsymbol{J}_{\mathrm{red}}^s$. Thus, we can focus on the case where $N'_s < N_s$. Without loss of generality, we may assume that the last column of $\boldsymbol{J}_s^{(l)}$ is a linear combination of the first $(l-1)$ columns of $\boldsymbol{J}_s^{(l)}$. This implies that $\boldsymbol{J}_s^{(l)} \tilde{\boldsymbol{v}}_l^s = \boldsymbol{0}$, i.e., $\tilde{\boldsymbol{v}}_l^s$ is in the null space of $\boldsymbol{J}_s^{(l)}$ and $\tilde{\boldsymbol{v}}_l^s \neq 0$. If $\boldsymbol{J}_s^{(l)} \tilde{\boldsymbol{v}}_l^s = \boldsymbol{0}$ and $l \neq N'_s$, we can reduce $\boldsymbol{J}_s^{(l)}$ to $\boldsymbol{J}_{\mathrm{sub}}^{(l-1)}$ by setting $\boldsymbol{v}_l^s \in \mathcal{V}_s$. Otherwise, we have $\boldsymbol{J}_s^{(l)} = \boldsymbol{J}_{\mathrm{red}}^s$ since $\boldsymbol{J}_s^{(l)}$ must be a full rank matrix. Conversely, $\boldsymbol{J}_s^{(l)}$ can be reconstructed from $\boldsymbol{J}_{\mathrm{sub}}^{(l-1)}$ if $\boldsymbol{v}_l^s$ is given. Specifically, we can define $\boldsymbol{j}_l \triangleq \boldsymbol{J}_{\mathrm{sub}}^{(l-1)} \boldsymbol{v}_l^s$ and $j_{l,l} \triangleq \boldsymbol{j}_l^T \boldsymbol{v}_l^s$ and they are sufficient to reconstruct $\boldsymbol{J}_s^{(l)}$. Hence, $\boldsymbol{v}_l^s$ can be interpreted as a certificate that $\boldsymbol{J}_s^{(l)}$ can be reduced to/reconstructed from $\boldsymbol{J}_{\mathrm{sub}}^{(l-1)}$ for $l = \{N'_s + 1, \ldots, N_s\}$. ∎

The proposed methods enable us to estimate N'_s for given N_1^s, N_2^s, W_1^s, and W_2^s. Furthermore, they allow us to verify that $\boldsymbol{J}_s$ indeed can be reduced to (or reconstructed from) $\boldsymbol{J}_{\mathrm{red}}^s$

with proof of certificates. An example of the estimations of N'_s is given in Table II. This table can help us better understand the performance of MIMO-FAS. For example, by substituting the estimation of N'_s into Theorem 1, we observe that MIMO-FAS yields massive diversity gains if $r < n_{\min}$. Thus, it is worth investigating how we can leverage MIMO-FAS effectively. To answer this question, we introduce the q-outage capacity.

Definition 1. The q-outage capacity of a system is defined as

$$C_{\mathrm{sys}}^q = q \left(1 - \bar{P}_{\mathrm{sys}}^{\mathrm{out}}(\mathrm{SNR}, q)\right), \qquad (45)$$

where

$$\bar{P}_{\mathrm{sys}}^{\mathrm{out}}(\mathrm{SNR}, q) = \mathbb{P}\{R_{\mathrm{sys}}(\mathrm{SNR}) < q\}, \qquad (46)$$

where $\bar{P}_{\mathrm{sys}}^{\mathrm{out}}(q)$ is the outage probability of a system for a fixed target rate or transmission rate q independent of the SNR. It is worth noting that (45) differs from the ϵ-outage capacity as it is not measuring the largest q such that $\bar{P}_{\mathrm{sys}}^{\mathrm{out}}(\mathrm{SNR}, q) \leq \epsilon$. Instead, (45) is interpreted as the average rate that a system can reliably transmit over period of time such that the statistics of the fading do not change. Furthermore, both q and $\bar{P}_{\mathrm{sys}}^{\mathrm{out}}(\mathrm{SNR}, q)$ play important roles in (45). For example, if $q \approx 0$, we usually have $\bar{P}_{\mathrm{sys}}^{\mathrm{out}}(\mathrm{SNR}, q) \approx 0$. If q is large, then we typically have $\bar{P}_{\mathrm{sys}}^{\mathrm{out}}(\mathrm{SNR}, q) \approx 1$. Nevertheless, both cases yield $C_{\mathrm{sys}}^q \approx 0$. In between the two extremes, we have $C_{\mathrm{sys}}^q \gg 0$ and there is an optimal q for a system such that (45) is maximized. In addition, the q-outage capacity gain of MIMO-FAS over a traditional antenna system can be characterized as

$$C_{\mathrm{MIMO\text{-}FAS}}^q - C_{\mathrm{sys}}^q$$
$$= q \left[\bar{P}_{\mathrm{sys}}^{\mathrm{out}}(\mathrm{SNR}, q) - \bar{P}_{\mathrm{MIMO\text{-}FAS}}^{\mathrm{out}}(\mathrm{SNR}, q)\right]. \quad (47)$$

Using (47), we can easily see the benefits that can be harnessed by MIMO-FAS over a traditional antenna system.

V. Results and Discussions

Here, we present the analytical and Monte Carlo simulation results to evaluate the performance of MIMO-FAS. For brevity, we focus on a symmetric MIMO-FAS design where $N_1^s = N_2^s$, $W_1^s = W_2^s$ and $W_{rx} = W_{tx}$. Unless stated otherwise, we assume that $N_s = 100$, $n_s = 4$, $W_s = 1\lambda^2$, $\delta_s^2 = 1$ and $\mathrm{SNR} = 30\mathrm{dB}$. We also consider multiple schemes based on different combinations of techniques to highlight the respective gains and effects. These benchmarking schemes are:[10]

- Optimal MIMO-FAS: It considers the MIMO-FAS setup that utilizes an exhaustive search, SVD and waterfilling for port selection, beamforming and power allocation, respectively.
- QR MIMO-FAS: This is the proposed MIMO-FAS that employs strong RRQR factorization, SVD and waterfilling power allocation for a suboptimal solution.

[10]Note that [23] has proposed a solution where the antennas can move to locally optimal positions. We can interpret these positions as activating some ports as $N_s \to \infty$. However, the solution cannot be employed here due to two impediments. Firstly, the spatial correlation of these positions cannot be obtained. Secondly, we are considering the cases where the positions might be discrete. Therefore, the solution is not considered in this paper.
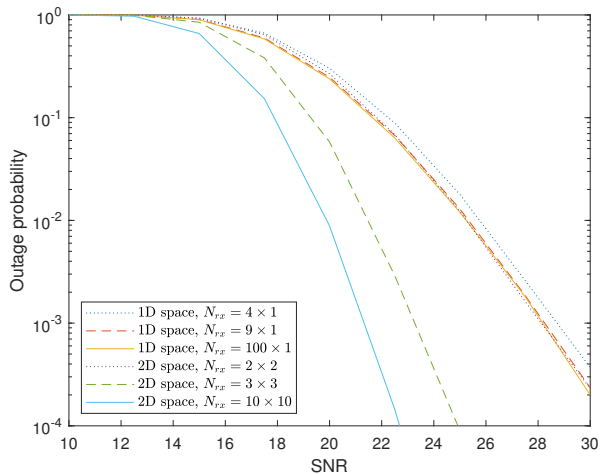
Figure 2: Outage probability of FAS versus SNR for different number of ports and dimensional space, with $q = 7\text{bps/Hz}$.

- Greedy MIMO-FAS: This is the MIMO-FAS that employs greedy selection, SVD and waterfilling power allocation for an efficient solution in the low SNR regime.
- Random MIMO-FAS: It randomly activates the ports and uses SVD as well as waterfilling power allocation.
- MIMO: This refers to the traditional MIMO that employs SVD and waterfilling power allocation. Unless otherwise stated, we assume that the number of antennas is $n_s^{\text{mimo}} = 4$ and the antennas are spatially correlated based on (1).
- MIMO-AS: This refers to the traditional MIMO antenna selection system that employs strong RRQR factorization, SVD and waterfilling power allocation. Unless stated otherwise, the number of active antennas is $n_s^{\text{mimo}-\text{as}} = 4$. Also, a maximum number of antennas is considered in the given surface where the antennas are placed based on a grid structure with at least half a wavelength apart, and they are spatially correlated due to (1).

To highlight the superiority of 2D space, we first consider a simplified scenario where there is only a single fluid antenna at the receiver. Fig. 2 shows the outage probability of FAS versus SNR for various number of ports and dimensional space. Here, the outage probability is obtained using (46) by replacing $R_{\text{sys}}(\text{SNR})$ with $R_{\text{QR}}(\text{SNR})$. Given the same number of ports, the ports that are distributed in 2D space can achieve a much lower outage probability as compared to the ones that are distributed in 1D space. This improvement can be explained from the fact that a 2D space has an additional dimension for the fluid antenna to move around. Hence, it contains more spatial diversity and yields a lower outage probability. This suggests that the ports in MIMO-FAS should be designed using the entire 2D space for better performance.

Next in Fig. 3, we study the average rates of the benchmarking schemes for different n_s at different SNR. Since the optimal MIMO-FAS is computed using an exhaustive search, we set $N_s = 12$ where $N_1^s = 3$ and $N_2^s = 4$. Fig. 3(a) illustrates that QR MIMO-FAS achieves a similar average rate as compared to the optimal MIMO-FAS at high SNR.
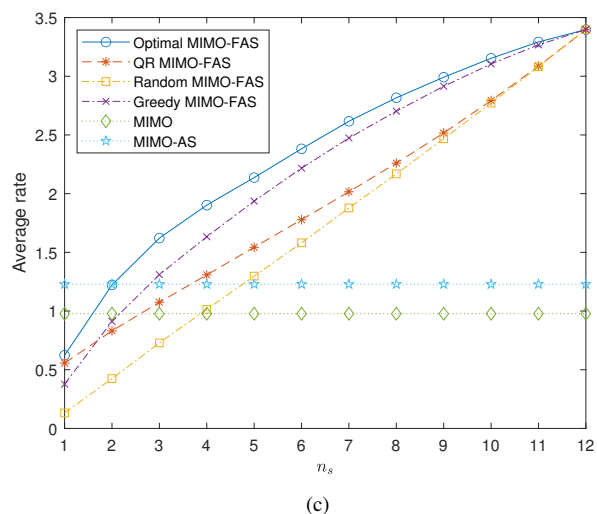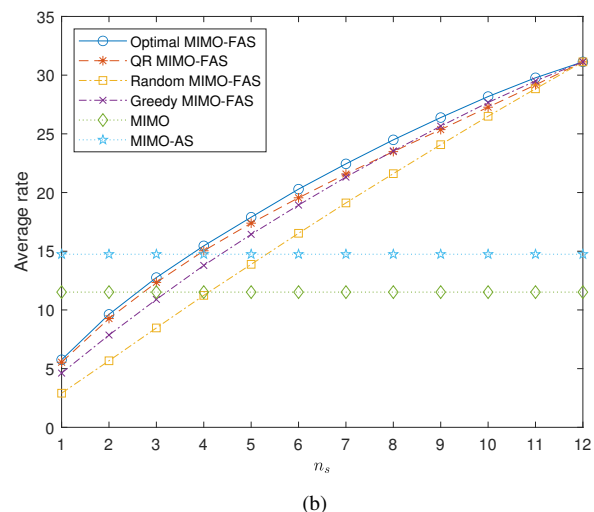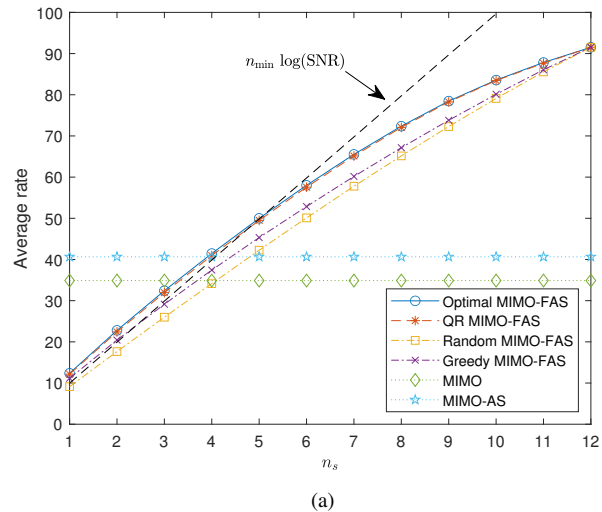

(a)

(b)

(c)

Figure 3: Average rates of the benchmarking schemes for different values of n_s: a) SNR = 30dB; b) SNR = 10dB; c) SNR = −10dB.

Furthermore, the average rate of QR MIMO-FAS scales like $n_s \log \text{SNR}$ when n_s ranges from 1 to 6. Nevertheless, it suffers from a diminishing rate gain when n_s ranges from 7 to 12. Thus, MIMO-FAS is most effective when each active port has the freedom of being at least half a wavelength apart from each other. In addition, the average rate of QR MIMO-FAS outperforms traditional MIMO when the number of active ports or antennas is the same (i.e., $n_s = 4$). This is because QR MIMO-FAS activates the optimal ports in each realization, which reduces the spatial correlation effect. In Fig. 3(b), we further observe that QR MIMO-FAS provides a higher sum-rate in the medium SNR regime when n_s is small while greedy MIMO-FAS yields a better performance when n_s is large. Nevertheless, as shown in Fig. 3(c), greedy MIMO-FAS is generally more efficient than QR MIMO-FAS in the low SNR regime. These results suggest that an efficient scheme with low complexity is still required to maximize the rate of MIMO-FAS in the medium and low SNR regimes. Besides, QR MIMO-FAS yields a similar or higher rate than MIMO-AS when the number of active ports or antennas is the same.

Fig. 4 presents the average rates and outage probabilities of the benchmarking schemes for different values of N_s. In these results, we omit the optimal MIMO-FAS because it is difficult to perform exhaustive search online for large N_s. On the other hand, since the activated ports can be placed very close to each other, it would be useful to consider the mutual coupling effect and investigate its effect on the performance of MIMO-FAS. In particular, we consider two designs: liquid-based and RF pixel-based fluid antennas. To make a fair comparison between the cases with and without mutual coupling, we assume that $N_1^s = \left\lfloor \frac{W_1^s}{0.5} \right\rfloor + 1$ and vary N_2^s accordingly. This means the resolution in one direction is fixed while we change the resolution of FAS in another direction to examine the impact of mutual coupling. The details of the mutual coupling model are given in Appendix III.

As seen in Fig. 4, generally speaking, the performance of QR MIMO-FAS and random MIMO-FAS with mutual coupling are not vastly different from the case without mutual coupling regardless of whether liquid-based or RF pixel-based fluid antenna is considered. This suggests that the active ports can be placed close to each other, typically much less than half a wavelength, and still yield a similar performance. By contrast, the rate performance of greedy MIMO-FAS appears to suffer more from mutual coupling as N_s increases. However, greedy MIMO-FAS is not supposed to work well here because the setting is under the high SNR regime.

It is worth pointing out that for RF pixel-based fluid antenna, mutual coupling can exist regardless of whether the pixels are on or off. It is therefore essential to improve the S-matrix via antenna design in order to achieve a good performance. However, the advantage of RF pixel-based fluid antenna is that the mutual coupling matrix is deterministic given N_1^s and N_2^s regardless of which pixels are the active ones. Thus, one can directly obtain the optimal port selection, beamforming and power allocation while taking into account of the mutual coupling effect. Moreover, matching networks can be employed directly to further improve the performance of MIMO-FAS but
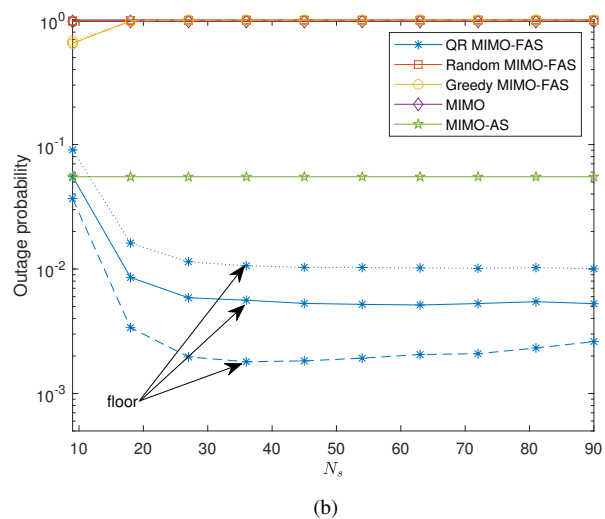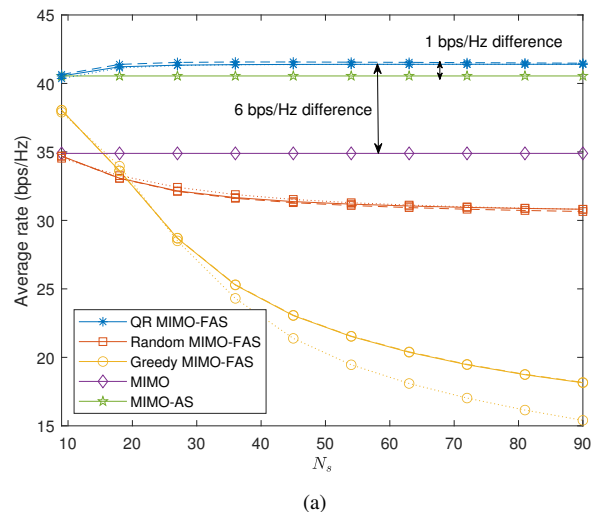

(a)

(b)

Figure 4: The performance of the benchmarking schemes for different values of N_s: (a) average rate; (b) outage probability, with $q = 39\text{bps/Hz}$; (solid) without mutual coupling; (dotted) liquid-based fluid antenna with mutual coupling; (dashed) RF pixel-based fluid antenna with mutual coupling.

this technique is not considered in our results.

Based on the above observations, we hence focus on the performance of MIMO-FAS without mutual coupling effect. In Fig. 4(a), we see that the average rates of random MIMO-FAS and greedy MIMO-FAS generally decrease as N_s increases. This suggests that efficient port selection in MIMO-FAS is essential. Furthermore, the average rate of QR MIMO-FAS is 1bps/Hz higher than that of MIMO-AS and 6bps/Hz higher than that of MIMO when N_s is large. In Fig. 4(b), the outage probabilities of random MIMO-FAS, Greedy MIMO-FAS and MIMO are near one (i.e., 0.99) while the outage probability of MIMO-AS is in the order of 10^{-2}. In contrast, the outage probability of QR MIMO-FAS is much lower (i.e., the order of 10^{-3}). Nevertheless, the outage probability of QR MIMO-FAS decreases to a floor as N_s continues to increase. This limitation is due to the fact that there are approximately $N_s^{'}$ diversity in
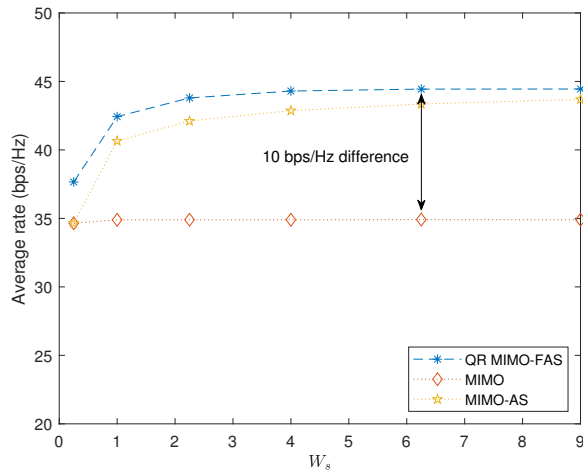
(a)
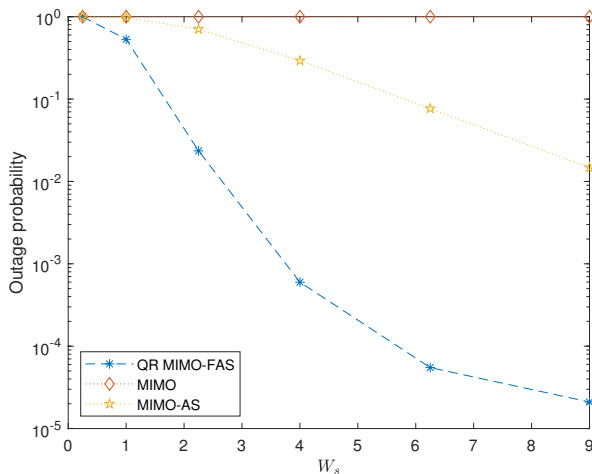
(b)

Figure 5: The performance of QR MIMO-FAS, MIMO and MIMO-AS for different values of W_s: (a) average rate; (b) outage probability, with $q = 42.5 \text{bps/Hz}$.

Figure 6: The outage probabilities of QR MIMO-FAS, MIMO and MIMO-AS for different values of q.
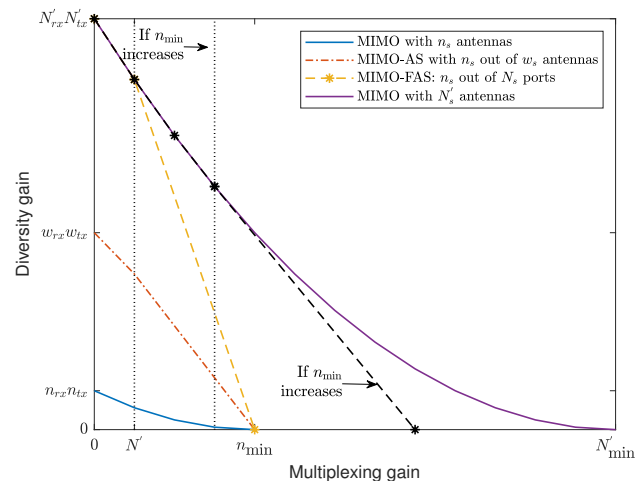
Figure 7: The optimal DMT of MIMO-FAS, MIMO and MIMO-AS.

J_s for a fixed W_s. Therefore, the outage probability of QR MIMO-FAS is limited by $N_s^{'}$ for a fixed W_s (see, Table II).

To verify this explanation, we further investigate the outage probabilities of QR MIMO-FAS, MIMO and MIMO-AS for different values of W_s. For brevity, we omit random MIMO-FAS and greedy MIMO-FAS as we now know that these schemes do not provide an effective performance for large N_s. As seen in Fig. 5(a), the average rates of QR MIMO-FAS, MIMO and MIMO-AS increase and then plateau. Nevertheless, as shown in Fig. 5(b), the outage probabilities of QR MIMO-FAS decrease without bound as W_s increases if N_s is sufficiently large. By analyzing Table II, we can observe that although N_s remains fixed, $N_s^{'}$ generally increases if W_s is increased. In contrast, the outage probability of MIMO is always near to being one since the diversity gain of MIMO remains the same even if W_s is increased. On the other hand, the outage probability of MIMO-AS decreases at a slower rate due to the lower resolution (i.e., the number of antennas is less
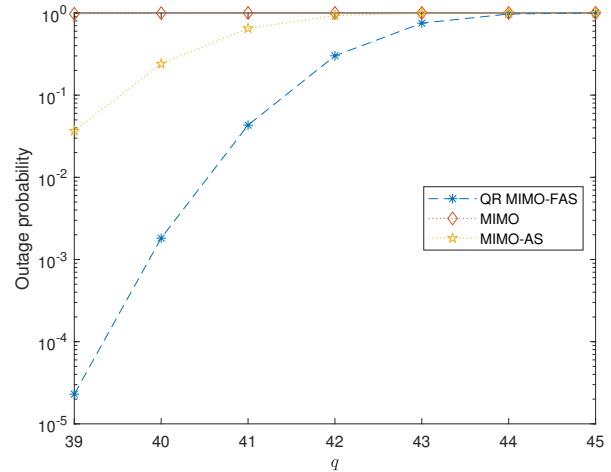
than the number of ports in the given space). Overall, Figs. 4 and 5 suggest that the value of N_s be determined by W_s.

From the above results, one might be amazed with the rate improvement of QR MIMO-FAS. Nevertheless, we highlight that the superiority of QR MIMO-FAS lies in the diversity gain. In particular, QR MIMO-FAS can reduce its outage probability to a much lower value than MIMO and MIMO-AS if q is low (e.g., $q < n_{\min} \log \text{SNR}$). To examine this phenomenon more closely, Fig. 6 illustrates the outage probabilities of QR MIMO-FAS, MIMO and MIMO-AS for different q. Within 6bits/Hz, we see that the outage probability of QR MIMO-FAS reduces at a steeper rate (e.g., from the order of 10^{-1} to 10^{-5}) while the outage probability of MIMO-AS reduces at a slower rate (e.g., from the order of 10^{-1} to 10^{-2}) and the outage probability of MIMO remains roughly the same.

To understand this at a more fundamental level, we present the DMT of QR MIMO-FAS in Fig. 7. Note that the DMT of QR MIMO-FAS is also the optimal DMT of MIMO-FAS. As
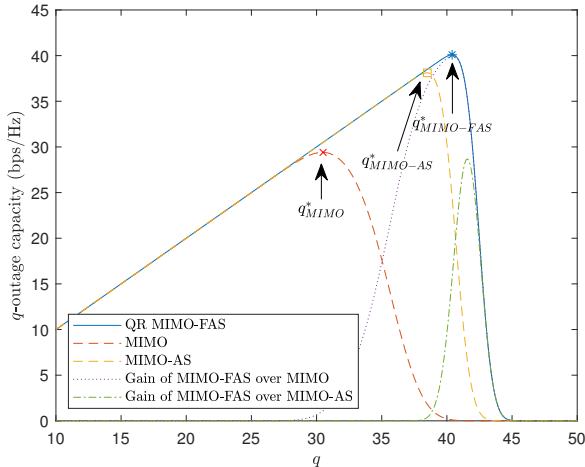
Figure 8: The q-outage capacity of MIMO-FAS, MIMO and MIMO-AS.

shown in Table II, the value of $N_s^{'}$ depends on W_s as long as $N_s \geq N_s^{'}$. In Fig. 7, it can be seen that the diversity gain of MIMO-FAS is much superior than that of an $n_{rx} \times n_{tx}$ MIMO system for a fixed r. For example, the maximum diversity of 4×4 MIMO is 16 as $r \to 0$. This is because the optimal DMT of a traditional $n_{rx} \times n_{tx}$ MIMO system is a piecewise linear function connecting the point $(r, (n_{rx} - r)(n_{tx} - r))$ [24]. Meanwhile, the maximum diversity of MIMO-AS is limited by $w_{rx}w_{tx}$. For instance, if $W_s = 1\lambda^2$, the maximum diversity of MIMO-AS is 81. In contrast, the maximum diversity gain of MIMO-FAS is approximately $23 \times 23 = 529 \gg \{81, 16\}$ if $W_{rx} = W_{tx} = 1\lambda^2$. Hence, the diversity gain of MIMO-FAS is massive because outage only occurs when all the ports experience deep fades. To obtain the same diversity gain at multiplexing gain r from 0 to N', a traditional $N_{rx}^{'} \times N_{tx}^{'}$ MIMO would have been required. However, the downside is that it can only have at most $n_{\min}$ multiplexing gain.

Finally, we investigate the q-outage capacity to showcase the benefits of MIMO-FAS. Fig. 8 presents the q-outage capacities of QR MIMO-FAS, MIMO and MIMO-AS as well as the q-outage capacity gain of QR MIMO-FAS over MIMO and MIMO-AS. For ease of exposition, the optimal q^* of QR MIMO-FAS, MIMO and MIMO-AS are denoted as $q^*_{\text{MIMO-FAS}}$, q^*_{MIMO}, $q^*_{\text{MIMO-AS}}$, respectively. As it is seen, the outage capacities of the schemes increase up to q^* and decrease thereafter. To the left side of q^*, the capacity is limited by q (i.e., rate) since $\bar{P}_{\text{sys}}^{\text{out}}(\text{SNR}, q)$ is small. To the right side of q^*, the capacity is limited by the outage probability because $\bar{P}_{\text{sys}}^{\text{out}}(\text{SNR}, q)$ is large. Since MIMO provides limited diversity gain and MIMO-AS has a limited number of antennas within a given space, both schemes fail to achieve certain q-outage capacity achievable by QR MIMO-FAS. This suggests that MIMO-FAS can reliably deliver a much higher rate than traditional MIMO and MIMO-AS systems.

VI. Conclusions

In this paper, we analyzed the performance limits of MIMO-FAS. To this end, we developed a system model for MIMO-

FAS where a 2D fluid antenna surface was used at both ends, while taking into account of the spatial correlation of the ports. We then proposed a suboptimal scheme to maximize the rate of MIMO-FAS at high SNR via joint port selection, beamforming and power allocation, namely QR MIMO-FAS. One key contribution was the derivation of the outer bound of the DMT for MIMO-FAS. Through the outer bound and the proposed scheme, we then obtained the optimal DMT of MIMO-FAS which revealed the fundamental limits of MIMO-FAS. Extensive results were presented, illustrating that QR MIMO-FAS achieved a similar rate as compared to the optimal MIMO-FAS in the high SNR regime. By fixing other MIMO-FAS parameters, we found that the average rate and outage probability of QR MIMO-FAS approached to a limit as N_s increased. Likewise, the average rate of QR MIMO-FAS improved up to a certain level as W_s increased. Nevertheless, the outage probability of QR MIMO-FAS decreased without bound as W_s increased. For the same multiplexing gain, we also showed that MIMO-FAS achieved massive diversity gain as compared to the traditional MIMO and MIMO-AS systems. Motivated by this, we further illustrated that MIMO-FAS could reliably deliver a much higher rate than the traditional MIMO and MIMO-AS systems in terms of q-outage capacity that jointly considered both rate and outage probability.

Appendix I: Spatial Correlation of 2D Fluid Antenna Surface over 3D Scattering Environment

Without loss of generality, let us refer to the position of the (n_1, n_2)-port as $\boldsymbol{n}_{l_s} = \left[0, \frac{n_2^s - 1}{N_2^s - 1}W_2^s, \frac{n_1^s - 1}{N_1^s - 1}W_1^s\right]^T$ where $\text{map}(n_1, n_2) = l_s$ and λ is the wavelength. Suppose a plane wave impinges on the fluid antenna surface from azimuth angle φ and elevation angle θ. Then, the array response vector can be expressed as [43]

$$\boldsymbol{a}(\varphi, \theta) = \left[e^{j\frac{2\pi}{\lambda}\boldsymbol{k}(\varphi,\theta)^T\boldsymbol{n}_1\lambda}, \ldots, e^{j\frac{2\pi}{\lambda}\boldsymbol{k}(\varphi,\theta)^T\boldsymbol{n}_{N_s}\lambda}\right]^T, \quad (48)$$

where

$$\boldsymbol{k}(\varphi, \theta) = \left[\begin{array}{ccc} \cos(\theta)\cos(\varphi) & \cos(\theta)\sin(\varphi) & \sin(\theta) \end{array}\right]^T, \quad (49)$$

is the normalized wave vector.

Let us denote the spatial correlation matrix as $\boldsymbol{J}_s = \mathbb{E}\left\{\boldsymbol{a}(\varphi, \theta)\boldsymbol{a}(\varphi, \theta)^H\right\}$. From (48), we know that the (k_s, l_s)-th entry of $\boldsymbol{J}_s$ can be expressed as

$$[\boldsymbol{J}_s]_{k_s, l_s} = \mathbb{E}\left\{e^{j\frac{2\pi}{\lambda}\boldsymbol{k}(\varphi,\theta)^T\boldsymbol{n}_{k_s}\lambda}e^{-j\frac{2\pi}{\lambda}\boldsymbol{k}(\varphi,\theta)^T\boldsymbol{n}_{l_s}\lambda}\right\}$$
$$= \mathbb{E}\left\{e^{j2\pi\boldsymbol{k}(\varphi,\theta)^T(\boldsymbol{n}_{k_s} - \boldsymbol{n}_{l_s})}\right\}, \quad (50)$$

where $\text{map}(\tilde{n}_1^s, \tilde{n}_2^s) = k_s$. Using the Jacobi-Anger plane wave expansion [44], (50) can be rewritten as

$$[\boldsymbol{J}_s]_{k_s, l_s} = 4\pi \sum_{m=0}^{\infty} \sum_{n=-m}^{m} (-i)^m \times$$
$$\alpha_m^n Y_m^n\left(\frac{\boldsymbol{n}_{k_s} - \boldsymbol{n}_{l_s}}{\|\boldsymbol{n}_{k_s} - \boldsymbol{n}_{l_s}\|}\right) \times$$
$$j_m\left(2\pi\|\boldsymbol{n}_{k_s} - \boldsymbol{n}_{l_s}\|\right), \quad (51)$$

where $j_m\left(.\right)$ is the spherical Bessel function of the first kind, $Y_m^n\left(\cdot\right)$ is the spherical harmonics, and

$$\alpha_m^n = \int_\Omega f_{\boldsymbol{k}(\varphi,\theta)}\left(\boldsymbol{k}\right) Y_m^n\left(\boldsymbol{k}\right) d\Omega\left(\boldsymbol{k}\right), \qquad (52)$$

where $\Omega\left(\boldsymbol{k}\right)$ is a surface element of a unit sphere Ω. For a 3D isotropic scattering environment, we have $f_{\boldsymbol{k}(\varphi,\theta)}\left(\boldsymbol{k}\right) = \frac{1}{4\pi}$ and thus (52) reduces to

$$\alpha_m^n = \frac{1}{4\pi}\int_\Omega Y_m^n\left(\boldsymbol{k}\right) d\Omega\left(\boldsymbol{k}\right). \qquad (53)$$

Using the fact that

$$Y_m^n\left(\frac{\boldsymbol{n}_{k_s} - \boldsymbol{n}_{l_s}}{\|\boldsymbol{n}_{k_s} - \boldsymbol{n}_{l_s}\|}\right) = \frac{1}{\sqrt{4\pi}} \quad \text{if } n = m = 0, \qquad (54)$$

and

$$\int_\Omega Y_m^n\left(\tilde{\boldsymbol{k}}\right) d\Omega\left(\tilde{\boldsymbol{k}}\right) = \begin{cases} \sqrt{4\pi} & \text{if } n = m = 0, \\ 0 & \text{otherwise,} \end{cases} \qquad (55)$$

(51) can be rewritten as

$$[\boldsymbol{J}_s]_{k_s,l_s} = j_0\left(2\pi\|\boldsymbol{n}_{k_s} - \boldsymbol{n}_{l_s}\|\right), \qquad (56)$$

which gives (1). Note that (1) conforms with [45]–[47] since $j_0\left(c\right) = \frac{\sin c}{c}$. In addition, (1) can be reduced to a 1D fluid antenna with 2D scattering environment by setting $N_1^s = 1$ and $\frac{0}{0} \triangleq 0$ and replacing $j_0\left(\cdot\right)$ by $J_0\left(\cdot\right)$ where $J_0\left(\cdot\right)$ is the Bessel function of the first kind [9].

APPENDIX II: GENERALIZATION TO OTHER SPATIAL CORRELATION MODELS

Without loss of generality, let us consider a 1D fluid antenna since a similar argument can be made for a 2D fluid antenna surface. To begin with, let us denote $\boldsymbol{J}$ as the $N \times N$ spatial correlation matrix. Suppose that $W \gg 0$, and the spatial correlation between the k-th port and the l-th port is $J_{k,l} = f\left(k, l, N\right)$ where the spatial correlation function f satisfies two conditions: i) $\lim_{N\to\infty} f\left(k, k \pm 1, N\right) = 1$ and ii) there are some $\exists l \neq k$ such that $f\left(k, l, N\right) \neq 1$. The first condition implies that the $\left(k \pm 1\right)$-th row/column of $\boldsymbol{J}$ can be removed from $\boldsymbol{J}$ since the $\left(k \pm 1\right)$-th row/column of $\boldsymbol{J}$ is always identical to the k-th row/column of $\boldsymbol{J}$ in the limit. The second condition implies that there exist some l-th port whose l-th row/column must be retained in $\boldsymbol{J}$ since its spatial correlation is completely distinct from the k-th port. If f satisfies these two conditions, then there must exist a minimal spacing c between the k-th and l-th ports such that their spatial correlation is distinct. Using the fact that W is finite, it is clear that there are at most $\bar{N}$ non-identical ports since conditions (i) and (ii) hold. In particular, $\bar{N}$ must be finite because $W \geq \bar{N}c > 0$. As a result, $\boldsymbol{J}$ can be rewritten as a symmetric $\bar{N} \times \bar{N}$ finite size matrix. Let us denote $N^{'}$ as the full rank of the symmetric $\bar{N} \times \bar{N}$ matrix where $N^{'} \leq \bar{N}$. Then, we can further reduce the symmetric $\bar{N} \times \bar{N}$ matrix to a full rank symmetric $N^{'} \times N^{'}$ submatrix $\boldsymbol{J}_{\text{red}}$ by removing the $\left(\bar{N} - N^{'}\right)$ dependent rows and columns. Consequently, $\boldsymbol{J}$ can be represented by $\boldsymbol{J}_{\text{red}}$ which is a full rank symmetric $N^{'} \times N^{'}$ finite-size matrix.

APPENDIX III: THE EFFECT OF MUTUAL COUPLING

In liquid-based fluid antenna, mutual coupling only occurs between the active ports. Thus, the MIMO-FAS channel with mutual coupling effect can be modeled as [48]

$$\bar{\boldsymbol{H}}_{mc} = \boldsymbol{Z}_{mc}^{rx,l} \bar{\boldsymbol{H}} \boldsymbol{Z}_{mc}^{tx,l}, \qquad (57)$$

where $\boldsymbol{Z}_{mc}^{rx,l}$ and $\boldsymbol{Z}_{mc}^{tx,l}$ are the mutual coupling matrices which can be pre-computed offline given the antenna technologies used. The mutual coupling matrix is given as

$$\boldsymbol{Z}_{mc}^{s,l} = (Z_A + Z_L)\left(\boldsymbol{Z}_s^l + Z_L\boldsymbol{I}\right)^{-1}, s \in \{rx, tx\}, \quad (58)$$

where Z_A, Z_L and $\boldsymbol{Z}_s^l$ are the antenna impedance, load impedance and mutual impedance matrix of the active ports, respectively. To compute $\boldsymbol{Z}_s^l$, we assume that each active port is a dipole element with a length of 0.5λ and a width of 0.001λ. Consequently, $Z_A = 73.08 + 42.21j$ and $Z_L = Z_A^*$. Due to the dipole's physical constraint, we fix $N_1^s = \left\lfloor \frac{W_1^s}{0.5} \right\rfloor + 1$ and vary N_2^s accordingly. If all the active ports are far from each other, we have $\boldsymbol{Z}_{mc}^s \approx \boldsymbol{I}$. Given (57), SVD and waterfilling power allocation are then performed. It is worth highlighting that this model is a conservative one because the mutual coupling effect is not considered when optimizing A_{tx} and A_{rx}. In fact, the performance of MIMO-FAS can be further improved when considering the mutual coupling effect and allowing the optimal active ports to be freely located within the given surface.

In RF pixel-based fluid antenna, mutual coupling can exist regardless of whether the pixels are on or off. Thus, in practice, it is important to improve the S-matrix via antenna design. To a coarse approximation, the S-matrix is modeled as

$$\boldsymbol{S}_{mc}^s = \begin{bmatrix} \alpha_{\text{rl}}S_{1,1}^s & \alpha_{\text{iso}}S_{1,2}^s & \cdots & \alpha_{\text{iso}}S_{1,N_s}^s \\ \alpha_{\text{iso}}S_{2,1}^s & \alpha_{\text{rl}}S_{2,2}^s & & \vdots \\ \vdots & & \ddots & \\ \alpha_{\text{iso}}S_{N_s,1}^s & \cdots & & \alpha_{\text{rl}}S_{N_s,N_s}^s \end{bmatrix}, \quad (59)$$

where α_{rl} and α_{iso} determine the improvement level of the return loss and isolation, respectively, while S_{k_s,l_s}^s is the S-parameter between the k_s-th and l_s-th ports. In this paper, we assume that the return loss and isolation levels are -15dB and 30dB, respectively, which are typical values that can be achieved using state-of-the-art technologies [49]. Given (59), the mutual impedance matrix of the RF pixel-based fluid antenna can be computed as

$$\boldsymbol{Z}_s^p = z_0\left(\boldsymbol{I} + \boldsymbol{S}_{mc}^s\right)\left(\boldsymbol{I} - \boldsymbol{S}_{mc}^s\right)^{-1}, \qquad (60)$$

where $z_0 = 50\Omega$ is the reference impedance. Similar to (58), the mutual coupling matrix is given as

$$\boldsymbol{Z}_{mc}^{s,p} = (Z_A + Z_L)\left(\boldsymbol{Z}_s^p + Z_L\boldsymbol{I}\right)^{-1}, s \in \{rx, tx\}. \qquad (61)$$

Similar to (57), the MIMO-FAS channel with mutual coupling effect is modeled as

$$\boldsymbol{H}_{mc} = \boldsymbol{Z}_{mc}^{rx,p} \boldsymbol{H} \boldsymbol{Z}_{mc}^{tx,p}. \qquad (62)$$

In contrast to (57) and (58), it is worth noting that (61) and (62) are $N_s \times N_s$ matrices. Given (62), the port selections,

beamforming and power allocation can be performed by different schemes. Note that matching networks can be employed to further improve the performance of MIMO-FAS [50].

REFERENCES

[1] F. Tariq *et al.*, "A speculative study on 6G," *IEEE Wireless Commun.*, vol. 27, no. 4, pp. 118–125, Aug. 2020.

[2] A. Shojaeifard *et al.*, "MIMO evolution beyond 5G through reconfigurable intelligent surfaces and fluid antenna systems," *Proc. IEEE*, vol. 110, no. 9, pp. 1244–1265, 2022.

[3] K. K. Wong, K. F. Tong, Y. Shen, Y. Chen, and Y. Zhang, "Bruce Lee-inspired fluid antenna system: Six research topics and the potentials for 6G," *Frontiers in Commun. and Netw., section Wireless Commun.*, 3:853416, Mar. 2022.

[4] Y. Huang, L. Xing, C. Song, S. Wang and F. Elhouni, "Liquid antennas: Past, present and future," *IEEE Open J. Antennas & Propag.*, vol. 2, pp. 473–487, 2021.

[5] A. Grau Besoli and F. De Flaviis, "A multifunctional reconfigurable pixeled antenna using MEMS technology on printed circuit board," *IEEE Trans. Antennas & Propag.*, vol. 59, no. 12, pp. 4413–4424, Dec. 2011.

[6] S. Song and R. D. Murch, "An efficient approach for optimizing frequency reconfigurable pixel antennas using genetic algorithms," *IEEE Trans. Antennas & Propag.*, vol. 62, no. 2, pp. 609–620, Feb. 2014.

[7] T. Ismail and M. Dawoud, "Null steering in phased arrays by controlling the elements positions," *IEEE Trans. Antennas & Propag.*, vol. 39, no. 11, pp. 1561–1566, Nov. 1991.

[8] S. Basbug, "Design and synthesis of antenna array with movable elements along semicircular paths," *IEEE Antennas Wireless Propag. Lett.*, vol. 16, pp. 3059–3062, Oct. 2017.

[9] K. K. Wong, A. Shojaeifard, K. F. Tong, and Y. Zhang, "Fluid antenna systems," *IEEE Trans. Wireless Commun.*, vol. 20, no. 3, pp. 1950–1962, Mar. 2021.

[10] K. K. Wong, A. Shojaeifard, K. F. Tong, and Y. Zhang, "Performance limits of fluid antenna systems," *IEEE Commun. Lett.*, vol. 24, no. 11, pp. 2469–2472, Nov. 2020.

[11] P. Mukherjee, C. Psomas and I. Krikidis, "On the level crossing rate of fluid antenna systems," in Proc. *IEEE Int. Workshop Signal Process. Advances Wireless Commun. (SPAWC)*, 4-6 Jul. 2022, Oulu, Finland.

[12] Z. Chai, K. K. Wong, K. F. Tong, Y. Chen, and Y. Zhang, "Port selection for fluid antenna systems," *IEEE Commun. Lett.*, vol. 26, no. 5, pp. 1180–1184, May 2022.

[13] L. Tlebaldiyeva, G. Nauryzbayev, S. Arzykulov, A. Eltawil, and T. Tsiftsis, "Enhancing QoS through fluid antenna systems over correlated Nakagami-m fading channels," in Proc. *IEEE Wireless Commun. & Netw. Conf. (WCNC)*, pp. 78–83, 10-13 Apr. 2022, Austin, TX, USA.

[14] L. Tlebaldiyeva, S. Arzykulov, K. M. Rabie, X. Li, and G. Nauryzbayev, "Outage performance of fluid antenna system (FAS)-aided Terahertz communication networks," in Proc. *IEEE Int. Conf. Commun. (ICC)*, 28 May-1 Jun. 2023, Rome, Italy.

[15] M. Khammassi, A. Kammoun and M.-S. Alouini, "A new analytical approximation of the fluid antenna system channel," *IEEE Trans. Wireless Commun.*, early access DOI:10.1109/TWC.2023.3266411.

[16] W. K. New, K. K. Wong, H. Xu, K. F. Tong and C.-B. Chae, "Fluid antenna system: New insights on outage probability and diversity gain," *IEEE Trans. Wireless Commun.*, early access, DOI:10.1109/TWC.2023.3276245.

[17] C. Skouroumounis and I. Krikidis, "Fluid antenna with linear MMSE channel estimation for large-scale cellular networks," *IEEE Trans. Commun.*, vol. 71, no. 2, pp. 1112–1125, Feb. 2023.

[18] L. Zhu, W. Ma, B. Ning, and R. Zhang, "Movable-antenna enhanced multiuser communication via antenna position optimization," [Online] arXiv preprint arXiv:2302.06978, 2023.

[19] K. K. Wong, and K. F. Tong, "Fluid antenna multiple access," *IEEE Trans. Wireless Commun.*, vol. 21, no. 7, pp. 4801–4815, Jul. 2022.

[20] N. Waqar, K. K. Wong, K. F. Tong, A. Sharples, and Y. Zhang, "Deep learning enabled slow fluid antenna multiple access," *IEEE Commun. Letters*, vol. 27, no. 3, pp. 861–865, Mar. 2023.

[21] K. K. Wong, K. F. Tong, Y. Chen, and Y. Zhang, "Fast fluid antenna multiple access enabling massive connectivity," *IEEE Commun. Lett.*, vol. 27, no. 2, pp. 711–715, Feb. 2023.

[22] H. Xu, K. K. Wong, W. K. New, and K. F. Tong, "On the outage probability for two-user fluid antenna multiple access," in Proc. *IEEE Int. Conf. Commun. (ICC)*, 28 May-1 Jun. 2023, Rome, Italy.

[23] W. Ma, L. Zhu and R. Zhang, "MIMO capacity characterization for movable antenna systems," *IEEE Trans. Wireless Commun.*, early access, DOI:10.1109/TWC.2023.3307696.

[24] L. Zheng and D. Tse, "Diversity and multiplexing: A fundamental tradeoff in multiple-antenna channels," *IEEE Trans. Inform. Theory*, vol. 49, no. 5, pp. 1073–1096, May 2003.

[25] K. K. Wong, K. F. Tong, and C. B. Chae, "Fluid antenna system-Part II: Research opportunities," *IEEE Commun. Lett.*, early access, DOI: 10.1109/LCOMM.2023.3284318.

[26] S. Sanayei and A. Nosratinia, "Antenna selection in MIMO systems," *IEEE Commun. Mag.*, vol. 42, no. 10, pp. 68–73, Oct. 2004.

[27] A. Goldsmith, S. Jafar, N. Jindal, and S. Vishwanath, "Capacity limits of MIMO channels," *IEEE J. Select. Areas Commun.*, vol. 21, no. 5, pp. 684–702, Jun. 2003.

[28] N. Iqbal, C. Schneider, and R. S. Thoma, "A fast and optimal deterministic algorithm for NP-Hard antenna selection problem," in Proc. *IEEE Int. Sym. Pers., Indoor, Mobile Radio Commun. (PIMRC)*, pp. 895–899, 30 Aug-2 Sep. 2015, Hong Kong, China.

[29] A. Civril and M. Magdon-Ismail, "On selecting a maximum volume sub-matrix of a matrix and related problems," *Theoretical Comp. Sci.*, vol. 410, no. 47, pp. 4801–4811, 2009.

[30] M. Gu and S. C. Eisenstat, "Efficient algorithms for computing a strong rank-revealing QR factorization," *SIAM J. Sci. Comp.*, vol. 17, no. 4, pp. 848–869, 1996.

[31] W. Ford, *Numerical linear algebra with applications: Using MATLAB*, Academic Press, 2014.

[32] N. Prasad and M. K. Varanasi, "Outage theorems for MIMO block-fading channels," *IEEE Trans. Inform. Theory*, vol. 52, no. 12, pp. 5284–5296, Dec. 2006.

[33] Z. Wang and G. Giannakis, "A simple and general parameterization quantifying performance in fading channels," *IEEE Trans. Commun.*, vol. 51, no. 8, pp. 1389–1398, Aug. 2003.

[34] L. Zhao, W. Mo, Y. Ma, and Z. Wang, "Diversity and multiplexing tradeoff in general fading channels," *IEEE Trans. Inform. Theory*, vol. 53, no. 4, pp. 1549–1557, Apr. 2007.

[35] Y. Jiang and M. K. Varanasi, "The RF-chain limited MIMO system-part I: Optimum diversity-multiplexing tradeoff," *IEEE Trans. Wireless Commun.*, vol. 8, no. 10, pp. 5238–5247, Oct. 2009.

[36] S.-G. Hwang, "Cauchy's interlace theorem for eigenvalues of Hermitian matrices," *The American Math. Monthly*, vol. 111, no. 2, pp. 157–159, 2004.

[37] H. Moon, "Waterfilling power allocation at high SNR regimes," *IEEE Trans. Commun.*, vol. 59, no. 3, pp. 708–715, Mar. 2011.

[38] A. Ghaderipoor, C. Tellambura, and A. Paulraj, "On the application of character expansions for MIMO capacity analysis," *IEEE Trans. Inform. Theory*, vol. 58, no. 5, pp. 2950–2962, May 2012.

[39] S. H. Simon, A. L. Moustakas, and L. Marinelli, "Capacity and character expansions: Moment-generating function and other exact results for MIMO correlated channels," *IEEE Trans. Inform. Theory*, vol. 52, no. 12, pp. 5336–5351, Dec. 2006.

[40] R. G. Gallager, *Principles of digital communication*, Cambridge University Press Cambridge, UK, vol. 1, 2008.

[41] L. Zheng and D. Tse, "Communication on the Grassmann manifold: A geometric approach to the noncoherent multiple-antenna channel," *IEEE Trans. Inform. Theory*, vol. 48, no. 2, pp. 359–383, Feb. 2002.

[42] P. C. Hansen, "The truncated SVD as a method for regularization," *BIT Numerical Math.*, vol. 27, pp. 534–553, 1987.

[43] E. Bjornson, J. Hoydis, L. Sanguinetti, *Massive MIMO networks: Spectral, energy, and hardware efficiency*, vol. 11. Now Foundations and Trends, 2017.

[44] R. Mehrem, "The plane wave expansion, infinite integrals and identities involving spherical Bessel functions," *Appl. Math. & Comp.*, vol. 217, no. 12, pp. 5360–5365, 2011.

[45] R. K. Cook, R. Waterhouse, R. Berendt, S. Edelman, and M. Thompson Jr, "Measurement of correlation coefficients in reverberant sound fields," *J. Acoustical Society of America*, vol. 27, no. 6, pp. 1072–1077, 1955.

[46] R. W. Heath Jr and A. Lozano, *Foundations of MIMO communication*, Cambridge University Press, 2018.

[47] E. Bjornson and L. Sanguinetti, "Rayleigh fading modeling and channel hardening for reconfigurable intelligent surfaces," *IEEE Wireless Commun. Lett.*, vol. 10, no. 4, pp. 830–834, Apr. 2021.

[48] C. T. Neil *et al.*, "On the performance of spatially correlated large antenna arrays for millimeter-wave frequencies," *IEEE Trans. Antennas & Propag.*, vol. 66, no. 1, pp. 132–148, Jan. 2018.

[49] A. C. K. Mak, C. R. Rowell and R. D. Murch, "Isolation enhancement between two closely packed antennas," *IEEE Trans. Antennas & Propag.*, vol. 56, no. 11, pp. 3411–3419, Nov. 2008.

[50] J. W. Wallace and M. A. Jensen, "Mutual coupling in MIMO wireless systems: A rigorous network theory analysis," *IEEE Trans. Wireless Commun.*, vol. 3, no. 4, pp. 1317–1325, Jul. 2004.

(Aven) Wee Kiat New received his Ph.D in Electrical Engineering from Universiti Teknologi Malaysia, M.Eng.Sc in Electrical Engineering from University of Malaya and B.IT in Data Communications and Networking from Multimedia University. He was a visiting researcher at Lancaster University and University of Cyprus. He is currently a research fellow at the Department of Electronic and Electrical Engineering, University College London, UK. His research interests are information theory, optimization, stochastic processes, machine learning and their applications in emerging areas of communications. He was the recipient of the 2021 IEEE Malaysia Comsoc/VTS best paper award, 2021 and 2020 IEEE Malaysia AP/MTT/EMC best paper awards.

(Kenneth) Kin-Fai Tong (M'99-SM'13-F'23) received the B.Eng. and Ph.D. degrees in electronic engineering from the City University of Hong Kong in 1993 and 1997, respectively. After graduation, Dr. Tong worked in the Department of Electronic Engineering at City University of Hong Kong as a Research Fellow. Two years later, he took up the post Expert researcher in the Photonic Information Technology Group and Millimetre-wave Devices Group at the National Institute of Information and Communications Technology (NiCT), Japan, where his main research focused on photonic-millimeter-wave planar antennas at 10GHz, 38 GHz and 60 GHz for high-speed wireless communications systems. In 2005, he started his academic career in the Department of Electronic and Electrical Engineering, UCL, as a lecturer. Now Dr. Tong is Chair in Antennas, Microwave and Millimeter-wave Engineering in the department. His current research interests include millimeter-wave and THz antennas, fluid antennas, 3D printed antennas and sub-GHz long range IoT networks. He served as the General Co-Chair of the 2017 International Workshop on Electromagnetics (iWEM), and Lead Guest Editor of IEEE OJAP in 2020.

(Kit) Kai-Kit Wong (M'01-SM'08-F'16) received the BEng, the MPhil, and the PhD degrees, all in Electrical and Electronic Engineering, from the Hong Kong University of Science and Technology, Hong Kong, in 1996, 1998, and 2001, respectively. After graduation, he took up academic and research positions at the University of Hong Kong, Lucent Technologies, Bell-Labs, Holmdel, the Smart Antennas Research Group of Stanford University, and the University of Hull, UK. He is Chair in Wireless Communications at the Department of Electronic and Electrical Engineering, University College London, UK.

His current research centers around 5G and beyond mobile communications. He is a co-recipient of the 2013 IEEE Signal Processing Letters Best Paper Award and the 2000 IEEE VTS Japan Chapter Award at the IEEE Vehicular Technology Conference in Japan in 2000, and a few other international best paper awards. He is Fellow of IEEE and IET and is also on the editorial board of several international journals. He is the Editor-in-Chief for IEEE Wireless Communications Letters since 2020.

Chan-Byoung Chae (S'06-M'09-SM'12-F'21) is an Underwood Distinguished Professor in the School of Integrated Technology, Yonsei University, Korea. Before joining Yonsei University, he was with Bell Labs, Alcatel-Lucent, Murray Hill, NJ, USA from 2009 to 2011, as a Member of Technical Staff, and Harvard University, Cambridge, MA, USA from 2008 to 2009, as a Postdoctoral Research Fellow. He received his Ph.D. degree in Electrical & Computer Engineering from The University of Texas at Austin in 2008. Prior to joining UT, he was a research engineer at the Telecommunications R&D Center, Samsung Electronics, Suwon, Korea, from 2001 to 2005.

He has been an Editor-in-Chief of the IEEE Trans. Molecular, Biological, and Multi-scale Communications (2019-2022) and a Senior Editor of the IEEE Wireless Communications Letters (2020-present). He has served/serves as an Editor for the IEEE Communications Magazine (2016-present), the IEEE Trans. on Wireless Communications (2012-2017), and the IEEE Wireless Communications Letters (2016-present). He is an IEEE ComSoc Distinguished Lecturer for the term 2020-2021 and 2022-2023.

He was the recipient/co-recipient of the CES Innovation Award in 2023, the IEEE ICC Best Demo Award in 2022, the IEEE WCNC Best Demo Award in 2020, the Best Young Engineer Award from the National Academy of Engineering of Korea (NAEK) in 2019, the IEEE DySPAN Best Demo Award in 2018, the IEEE/KICS Journal of Communications and Networks Best Paper Award in 2018, the IEEE INFOCOM Best Demo Award in 2015, the IEIE/IEEE Joint Award for Young IT Engineer of the Year in 2014, the KICS Haedong Young Scholar Award in 2013, the IEEE Signal Processing Magazine Best Paper Award in 2013, the IEEE ComSoc AP Outstanding Young Researcher Award in 2012, the IEEE VTS Dan. E. Noble Fellowship Award in 2008.

Hao Xu (S'15 – M'19) received the B.S. degree in communication engineering from Nanjing University of Science and Technology, Nanjing, China, in 2013, and the Ph.D. degree in information and communication engineering with the National Mobile Communications Research Laboratory, Southeast University, Nanjing, China, in 2019. From 2019 to 2021, he was an Alexander von Humboldt (AvH) Post-Doctoral Research Fellow with the Faculty of Electrical Engineering and Computer Science at the Technical University of Berlin, Germany. He is currently a Marie Sklodowska-Curie Actions (MSCA) Individual Fellow with the Department of Electronic and Electrical Engineering, University College London, UK. His research interests mainly include information theory, mathematical optimization, MIMO systems, and physical layer security in wireless networks.